

Cite this: *J. Mater. Chem. A*, 2023, **11**, 9721

# Multidimensional MOF-derived carbon nanomaterials for multifunctional applications

Shaojie Xu,<sup>a</sup> Anrui Dong,<sup>a</sup> Yue Hu,<sup>a</sup> <sup>a</sup> Zhi Yang,<sup>a</sup> Shaoming Huang <sup>b</sup> and Jinjie Qian <sup>\*a</sup>

Currently, porous metal–organic frameworks (MOFs) have become popular precursors for the construction of new nanomaterials as a result of their large surface area, high porosity, and excellent chemical, mechanical and thermal stability. Among them, pyrolyzed MOF-derived porous carbon nanomaterials (CNMs) can well inherit the characteristics and advantages of the MOF precursors, and show great application prospects in the fields of environment and energy. More and more MOF-derived CNMs have been reported, but there is no systematic method to classify and summarize them. Based on this situation, we are going to classify the types of MOF-derived CNMs from the perspective of dimension, and comprehensively introduce the research progress of controlled synthesis of such materials in recent years. This review focuses on the changes in the morphology and phase composition of MOF-derived CNMs from the selection of MOF precursors to the final material carbonization process. The progress of MOF-derived CNMs in popular applications, including heterogeneous catalysis, fuel cells, sensor components, and so on, is systematically introduced. The influence of material morphology and composition on the performance is emphatically analyzed.

Received 13th January 2023  
Accepted 20th March 2023

DOI: 10.1039/d3ta00239j

rsc.li/materials-a

## 1. Introduction

Porous metal–organic frameworks (MOFs) are an emerging subclass of crystalline organic–inorganic hybrid materials, which are structurally constructed based on versatile

coordination bonds between organic ligands and inorganic metals.<sup>1,2</sup> As early as in the 1990s, Omar M. Yaghi proposed to select appropriate rigid organic ligands and metal ions to construct microporous materials, that are MOFs, and then introduced the famous MOF-5, which set off a hot MOF research craze. After that, similar materials such as HKUST-1, ZIF, MIL, UiO, *etc.* were reported successively in the following two decades and showed great application potential. The advantages of large specific surface area, high porosity, and excellent chemical, mechanical and thermal stability make MOF materials popular precursors for building new nanomaterials.<sup>3–5</sup> In the meantime,

<sup>a</sup>Key Laboratory of Carbon Materials of Zhejiang Province, College of Chemistry and Materials Engineering, Wenzhou University, Wenzhou 325035, Zhejiang, P. R. China. E-mail: jinjieqian@wzu.edu.cn

<sup>b</sup>School of Materials and Energy, Guangdong University of Technology, Guangzhou 510006, Guangdong, P. R. China



Shaojie Xu received his bachelor's degree from Wenzhou University, and he is now a graduate student at Wenzhou University. His current research is mainly focused on the facile synthesis of crystalline MOFs and MOF-derived carbon/oxide nanomaterials for green electrocatalytic applications, including the oxygen/hydrogen evolution reaction.



Dr Jinjie Qian received his PhD degree in 2015 from the Fujian Institute of Research on the Structure of Matter (FJIRSM), Chinese Academy of Sciences, under CAS Academician Mao-chun Hong. He is an associate professor at the College of Chemistry and Materials Engineering, Wenzhou University. His current research involves the electrochemical research on the nanostructures and adjustable

morphology of metal–organic frameworks as well as their derivatives for energy applications.

they have attracted much attention on account of their diverse and tunable nanostructures, and have been proven to be used as hierarchically porous derivatives with rich properties across industry and research fields.<sup>6,7</sup> On the other hand, the inherent instability and low electrical conductivity of MOFs have led to an interest in alternatives to metal-based derivatives derived from MOFs, which can retain the complex nanostructures of MOFs while exhibiting several orders of magnitude higher stability and conductivity, further broadening the application of MOF materials. They mainly consist of MOF-derived metal oxides, nitrides, phosphides, sulfides, selenides and transition metal-modified porous carbon nanomaterials (CNMs).<sup>8–10</sup> Most of the MOF derivatives inherit the characteristic advantages of their precursors to a large extent, where they not only achieve the structural stability and tunability but also ensure the high dispersion of active sites.<sup>11</sup> Under these circumstances, the rational design of MOF nanostructures and the facile transformation control of their derivatives are of great significance, which further determines their use in a wide range of practical applications.

On the other hand, carbon materials stand out as one of the key engineering materials in the application of science and technology. The highly sp<sup>2</sup>-hybridized graphitic CNMs are structurally stable under working conditions, and their electronic properties, such as band gap adjustment and excellent electrical conductivity, make them popular in terms of material selection.<sup>12,13</sup> It is worth mentioning that the high electron density generated by the Fermi level of the unique state occurring at the edge of the nanosized graphitic carbon is generally regarded as the source of its real chemical activity.<sup>14–16</sup> There are a variety of preparation methods, such as physical or chemical carbonization of carbon materials, the template method using mesoporous silica and zeolite, the high-temperature solvothermal and hydrothermal method, the traditional arc method, chemical vapor decomposition (CVD), and the relatively flexible and simple carbonization method using an organic precursor.<sup>17,18</sup> However, the low surface area, irregular size and disordered structure of these conventional carbon derivatives greatly restrict their development and application.<sup>19–21</sup> Theoretically speaking, multifunctional CNMs stemming from porous MOF precursors can perfectly overcome these above limitations and take the lead in precise applications.<sup>22–24</sup>

In these pioneering studies, some CNMs have been prepared by introducing carbon precursors into the MOF nanopores, while the direct carbonization of MOFs has recently become the mainstream choice.<sup>25–27</sup> The main reason is that MOF-derived CNMs could effectively maintain the structural features of MOF materials, such as high porosity, large specific surface area, high structural stability, and uniformly dispersed active sites.<sup>27,30–32</sup> To date, researchers have been committed to improving their application performance from the initial selection of metal and ligands to the subsequent carbon synthesis.<sup>28–30</sup> First of all, metal cations are linked to ligand molecules in MOFs, and their coordination configuration determines the arrangement and positioning of ligands.<sup>31–33</sup> Choosing appropriate bridging ligands will lead to

a coordination polymer with the expected orientation, structure, topology and properties.<sup>34–36</sup> Secondly, as a catalyst and carbon source in the carbonization process, the catalytic effect of metals on carbon formation and the double-sided effect of MOF derivatives generated by ligand decomposition on the resultant CNMs should be fully considered.<sup>37–39</sup> Last but not least, the sintering phenomenon of MOFs, agglomeration of metal nanoparticles (NPs), and disordered/ordered bonding of carbon materials all have a significant impact on the morphology of CNMs, thus affecting their practical structure–activity relationship.<sup>40–42</sup> Therefore, it is necessary to perform an in-depth study of the morphology and component forming mechanism, and summarize the theory and guide the preparation of multifunctional MOF-derived CNMs.

What is troubling is that despite the proliferation of MOF-derived CNMs, there is no systematic and comprehensive way to integrate them. After reviewing a series of studies on the preparation and applications of MOF-derived CNMs, we have carefully analyzed their similarities and differences, and proposed a classification from the perspective of material dimensionality: ① zero dimensional (0D): porous MOFs will reduce their dimensionality and form simple 0D carbon materials after carbonization, including a pure metal or alloy coated with multi-layer graphitic carbon shells.<sup>43,44</sup> ② One dimensional (1D): carbon nanotubes (CNTs) are the most famous 1D multifunctional carbons. Experimentally, versatile MOFs act as catalysts, carbon sources, templates and carriers in the process of carbonization and growth of CNTs. In addition, carbon nanorods, carbon nanowires, and carbon nanofibers with linear nanostructures and high aspect ratios are also classified as 1D CNMs.<sup>45,46</sup> ③ Two dimensional (2D): typical 2D graphene can be prepared by oxidation processes, mechanical or chemical stripping, plasma etching, top-down organic synthesis, and epitaxial growth. Similarly, porous crystalline MOFs provide suitable precursors or templates for the facile preparation of 2D graphitic carbons.<sup>47–50</sup> ④ Three dimensional (3D): here, we classify and define the unique porous carbon calcined from MOFs as 3D CNMs, but not limited to 3D polyhedral carbons, core–shell carbons, and hollow carbons (Scheme 1).<sup>51–53</sup>

During the past three decades, there has been an explosive development of MOF materials. Because the coordination environment within MOFs is relatively stable, MOF-derived CNMs partially retain the structural characteristics of the precursors during pyrolysis. MOFs of different sizes and morphological features can be efficiently transformed into well-defined nanostructures with different dimensions by *in situ* as well as *ex situ* preparation methods. In recently reported studies, under the conditions of a self-supporting MOF-assisted strategy, the introduction of different dimensions of metal–carbon nanocomposites into multidimensional structural materials has been becoming a hot topic. Based on the classification of CNMs from MOFs, the latest progress of their synthesis strategies, formation mechanisms and structural advantages is summarized in this review. Furthermore, there are numerous reports on MOF-derived CNMs applied widely in different application areas, such as catalysis, energy, environment and detection. Finally, the key challenges and prospects of



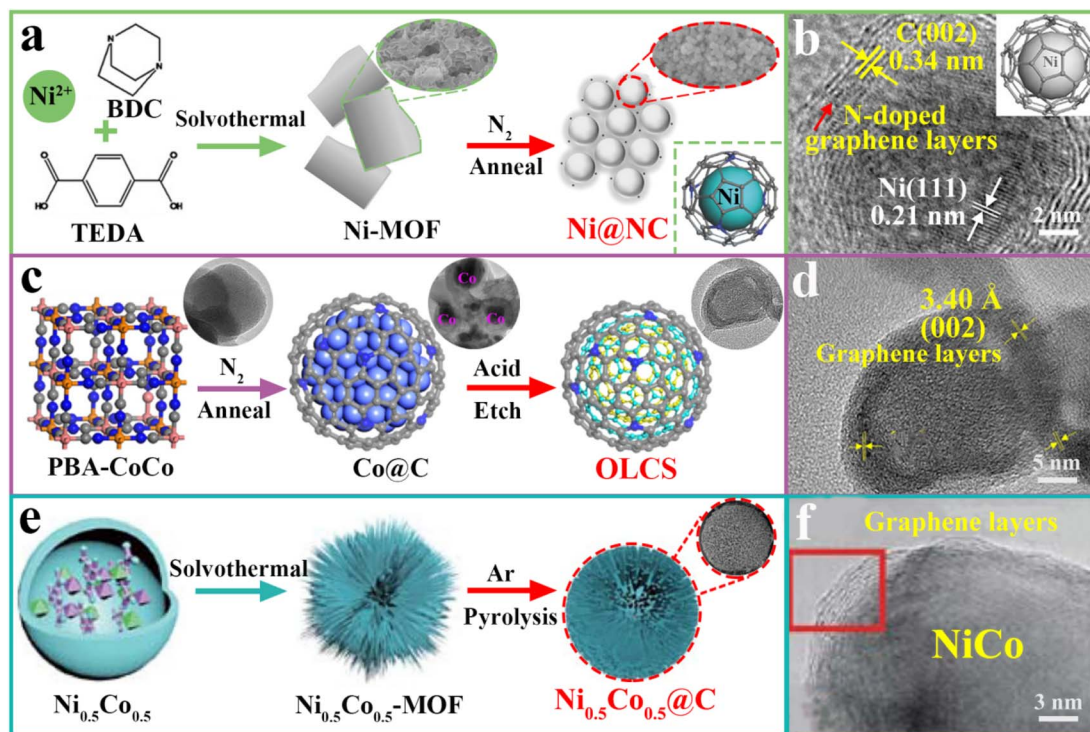


**Fig. 1** (a), (c), and (e) Routes to obtain MOF-derived 0D Ni@NC, OLCS and Ni<sub>0.5</sub>Co<sub>0.5</sub>@C, respectively; (b), (d) and (f) HRTEM images of Ni@NC-800, OLCS and Ni<sub>0.5</sub>Co<sub>0.5</sub>@C, respectively. [(a) and (b)] reproduced with permission from ref. 62, copyright© 2017, WILEY-VCH Verlag GmbH & Co. KGaA, Weinheim; [(c) and (d)] reproduced with permission from ref. 63, copyright© 2019, Elsevier B. V.; [(e) and (f)] reproduced with permission from ref. 64, copyright© 2020, W. Lei *et al.*

Therefore, by selecting suitable inorganic metals and organic linkers, 0D carbon nanocages can be accurately obtained from prefabricated MOFs, that also provide inspiration for the subsequent development of multidimensional as well as multifunctional carbon nanostructures.

## 2.2. MOF-derived 1D carbon materials

In past reports, multifunctional CNMs with a single nanostructure cannot meet the demands of further practical applications, and most of them are based on the growth of higher dimension carbon materials to maximize their real roles.<sup>73–75</sup> From the perspective of the formation principle and material morphology, herein, we have defined CNTs, carbon nanofibers and carbon nanorods with an obviously linear morphology as 1D carbons. Among them, CNTs, as typical 1D radial nanosized carbons, are structurally featured with remarkable mechanical, chemical, electrical and optical properties,<sup>76–78</sup> while porous MOF precursors possess a unique pore structure and controllable space for the facile preparation of CNTs. In this case, the desired 1D CNMs can be well synthesized by the *in situ* growth method using the intrinsic conditions of the MOF itself and the *ex situ* growth method with the help of external factors, including a catalyst, carbon sources, *etc.*<sup>79–81</sup> Similarly, these MOF-derived 1D carbon nanofibers and carbon nanorods also play the role of 1D CNMs on account of their similarity in structure and morphology.

**2.2.1. Carbon nanotubes (*in situ* growth).** Generally speaking, the *in situ* growth of CNTs from porous metal–organic coordination polymers has been a popular research topic in recent years. Owing to the advantages of good controllability, structural tunability, and ease of mass production, versatile MOF materials are currently becoming the first choice for the convenient syntheses of 1D CNMs.<sup>82–84</sup> First of all, MOF materials are considered to be good autocatalytic precursors structurally constituting metals and carbon sources. During the carbonization process, CNTs could be effectively catalyzed from mono-metals, polymetallic alloys and metal carbides with carbon solubility according to the gas–liquid–solid theory.<sup>85–87</sup> Secondly, the abundant and large pore structure in MOFs can carry external catalysts, allowing space limitation in the process of calcination, and providing infinite possibilities for the thermal conversion of crystalline MOFs into multi-walled or single-walled CNTs. Finally, the thermal treatment of MOF materials contributes to the activation of metal-based catalysts and organic components, and provides favorable conditions for the recombination of carbon species to form CNTs as a result of the spatial confinement effect and the energy released during the breaking of coordination bonds.<sup>88–91</sup>

Under the conditions of carbonization at high temperatures, the ligands of MOFs can be used as the only carbon source to efficiently grow CNTs *in situ* while maintaining the original morphology. As is known to all, highly graphitic multi-walled CNTs endow these MOF derivatives with high electrical

conductivity. Su *et al.* demonstrated a unique  $\text{Cu}_3\text{P}/\text{Cu}$  encapsulated by a CNT-assembled hierarchical octahedral carbonaceous matrix ( $\text{Cu}_3\text{P}/\text{Cu}@\text{CNHO}$ ) from Cu-MOF octahedra (Fig. 2a).<sup>92</sup> Its structural features are further characterized by SEM/(HR)TEM images to reveal a relatively rough surface anchored by autogenic CNTs (Fig. 2b–d). In addition, the finely designed MOF-on-MOFs with diverse structures and compositions can also be a good carrier for the *in situ* growth of 1D carbon materials. As shown in Fig. 2e, Li *et al.* synthesized one core-shell ZIF-8@ZIF-67 that can be easily converted into a N-doped CNT hollow polyhedron (NCNHP) followed by carbonization.<sup>93</sup> After phosphorization, hollow polyhedra of CoP/NCNHP composed of CNTs and CoP are also preserved with high porosity (Fig. 2f–h). In Fig. 2i–m, a similar process from leaf-shaped core-shell ZIF-L@ZIF-67 is demonstrated, which is

then pyrolyzed to give Co,N-doped porous carbon leaves (Co,N-PCL) with numerous CNTs.<sup>94</sup> Inspired by the above considerations, our group had also prepared hierarchical CoP-InNC@CNT with CoP NPs embedded into CNTs and N-doped carbon from the pre-designed InOF-1@ZIF-67 (Fig. 2n).<sup>95</sup> In this case, the obtained MOF-on-MOF precursor is pyrolyzed at 800 °C in Ar or  $\text{Ar}/\text{H}_2/\text{C}_2\text{H}_4$  to obtain MOF-derived 1D carbons, which clearly show the rough surface of CoInNC@CNT inherently anchored to a large number of CNTs in Fig. 2o–r.

**2.2.2. Carbon nanotubes (*ex situ* growth).** Compared with direct growth without any additives, the *ex situ* growth strategy can precisely control the growth and even the morphology of CNTs in specific steps.<sup>96,97</sup> Yang *et al.* prepared sea urchin-like multi-shelled hollow microspheres composed of N-doped CNTs covered with NiS NPs, denoted as NiS@NCNT MSHMs

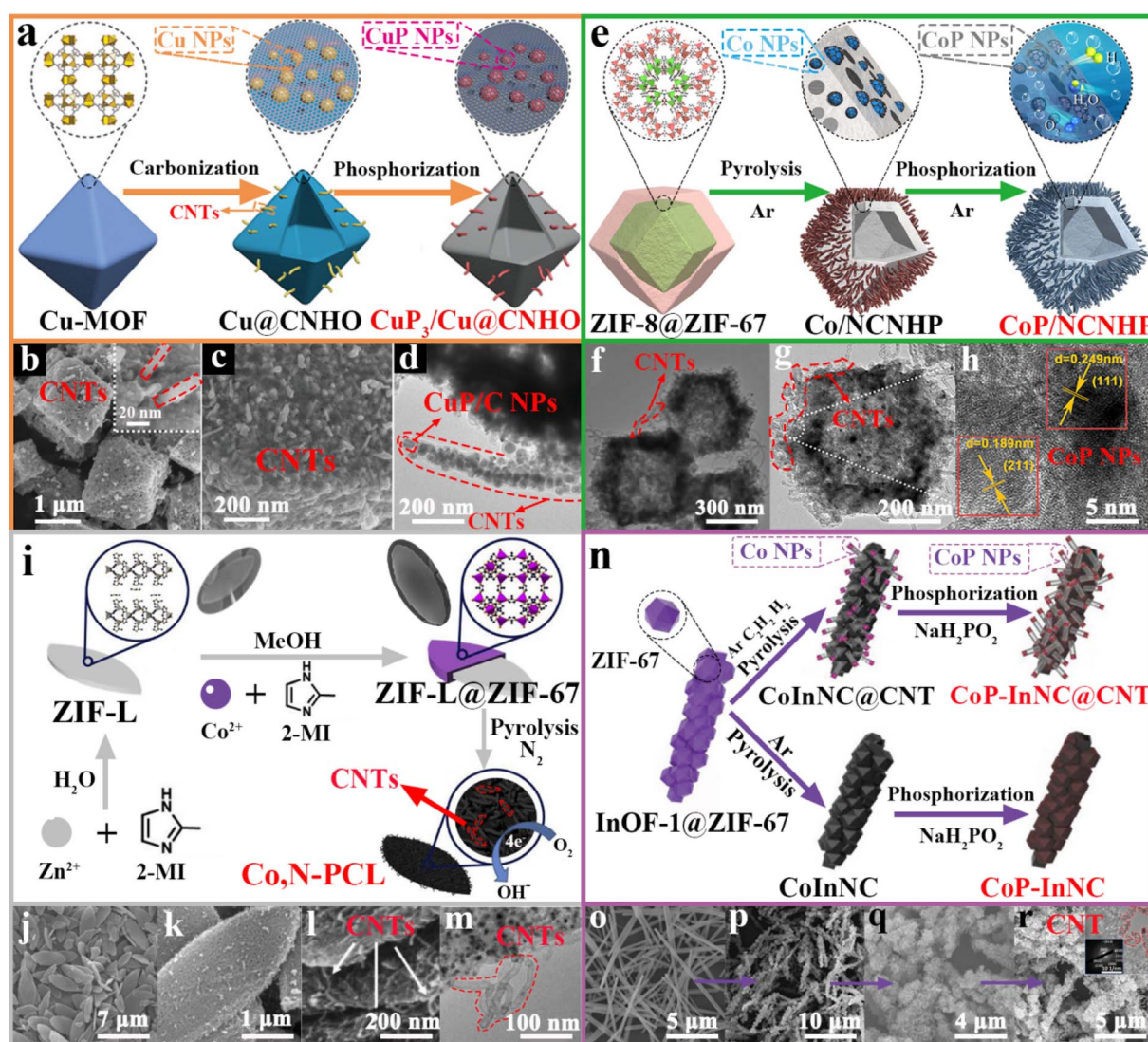
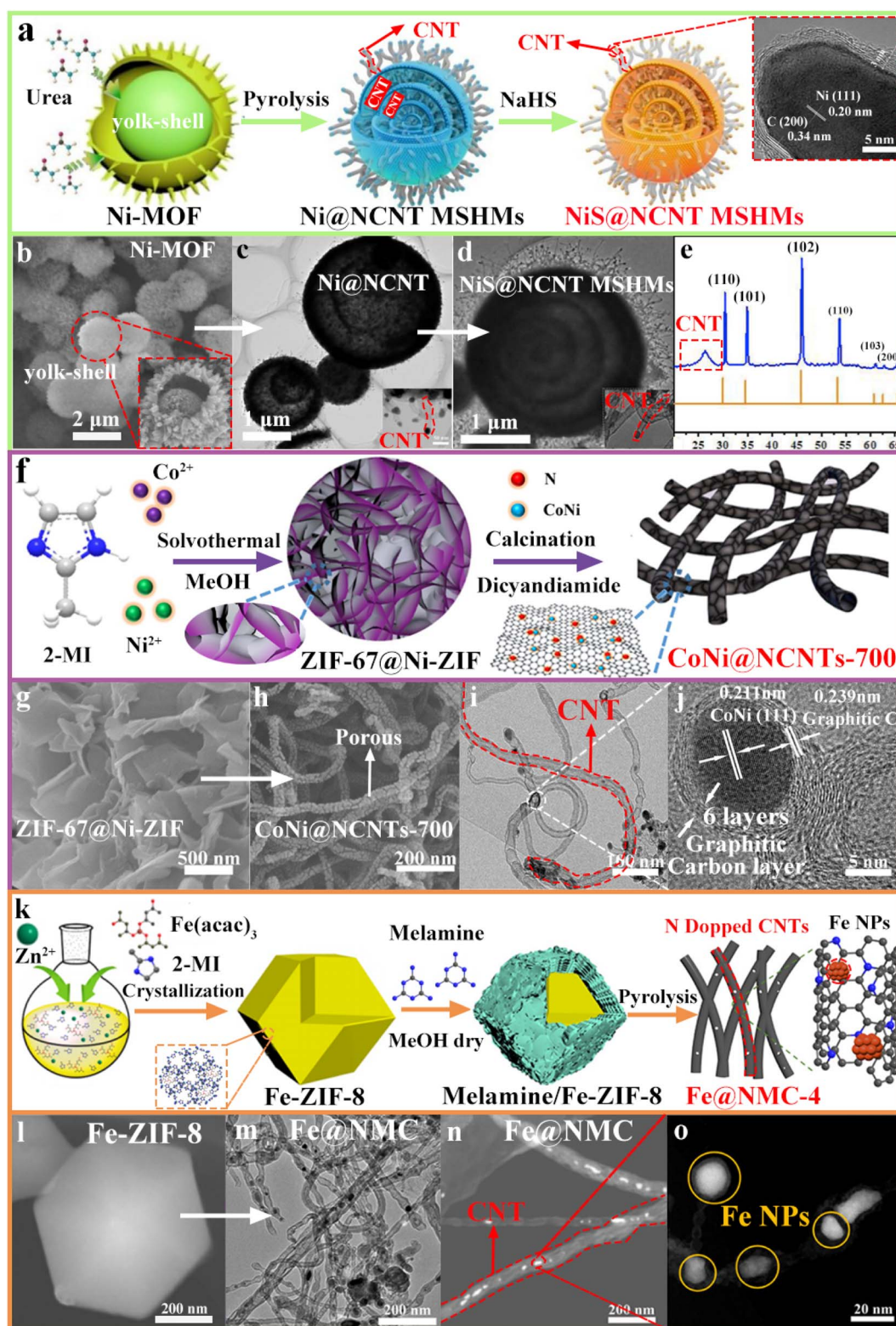


Fig. 2 (a), (e), (i) and (n) Schematic syntheses of MOF-derived 1D CNTs for  $\text{Cu}_3\text{P}/\text{Cu}@\text{CNHO}$ , CoP/NCNHP, Co,N-PCL, and CoP-InNC@CNT; SEM/(HR)TEM images of (b)–(d)  $\text{Cu}_3\text{P}/\text{Cu}@\text{CNHO}$  [(a)–(d)] reproduced with permission from ref. 92, copyright© 2020, WILEY-VCH Verlag GmbH & Co. KGaA, Weinheim); (f)–(h) CoP/NCNHP [(e) reproduced with permission from ref. 93, copyright© 2018, American Chemical Society); (j)–(m) Co,N-PCL [(i) reproduced with permission from ref. 94, copyright© 2019, Elsevier B. V.); (o and r) InOF-1@ZIF-67 and its derivatives [(n) reproduced with permission from ref. 95, copyright© 2020, WILEY-VCH Verlag GmbH & Co. KGaA, Weinheim).



**Fig. 3** (a), (f) and (k) Schematic synthesis processes of MOF-derived 1D CNTs for NiS@NCNT MSHMs, CoNi@NCNTs and Fe@NMC-4, respectively; (b)–(d) SEM/TEM images of Ni-MOF, Ni@NCNT, and NiS@NCNT MSHMs; (e) XRD patterns ([a]–[e]) reproduced with permission from ref. 98, copyright© 2019, Elsevier B. V.); (g)–(j) SEM/TEM images of ZIF-67@Ni-ZIF nanosheets and CoNi@NCNTs-700 ([f]–[j]) reproduced with permission from ref. 99, copyright© 2020, Elsevier B. V.); (l)–(o) TEM and HAADF-STEM images for Fe-ZIF-8 derived Fe@NMC-4 ([k]–[o]) reproduced with permission from ref. 100, copyright© 2019, American Chemical Society).

(Fig. 3a).<sup>98</sup> In this case, nickel nitrate and trimesic acid are used as the metal source and organic ligand, respectively, to synthesize egg yolk-shell Ni-MOFs (Fig. 3b). Secondly, unvulcanized Ni@NCNT MSHMs composed of NCNTs and Ni NPs are obtained by carbonizing Ni-MOF precursors together with urea, which are subjected to a simple vulcanization process to form well-preserved NiS@NCNT MSHMs (Fig. 3c and d). Furthermore, the sharp peaks in powder XRD patterns are well attributed to NiS, while the broad peak at 26.1° corresponds to CNTs (Fig. 3e). Similarly, Wang's group first synthesized ZIF-67@Ni-ZIF nanosheets, and then added dicyandiamide to obtain CoNi@NCNTs (Fig. 3f).<sup>99</sup> It would capture the volatile CN<sub>x</sub> species decomposed from external dicyandiamide so that nitrogen could be easily doped to form active CoNi-N<sub>x</sub> and porous CNTs. As discussed earlier, both metallic Co and Ni act as catalysts to promote the conversion of carbon sources into thin-layer graphitic CNTs, where CoNi alloys are anchored on the surface of hollow CNTs (Fig. 3g-j). Furthermore, 1D Fe@NMC-x series were also prepared by pyrolysis of regular rhombic dodecahedral Fe-ZIF-8 particles with melamine (Fig. 3k).<sup>100</sup> During calcination, Fe atoms coordinate with N species, and the released NH<sub>3</sub> gases attack the coordination bond and promote the formation of an inner cavity. Because of the efficient catalysis of *in situ* formed Fe NPs, a large number of interwoven CNTs are generated when excess melamine is added (Fig. 3l-o).

In principle, it is highly possible to prepare 1D CNTs by using co-existing catalysts with high catalytic activity and sufficient carbon sources under appropriate pyrolysis conditions. To explain the general mechanism of CNT growth, metal atoms (either already available in the MOF itself or introduced externally) are first polymerized at high temperatures to form thermodynamically stable catalysts. In this case, the metal-based species have ultra-high surface energy, while these coordinated ligands or external sources are then thermally decomposed into carbon fragments and adsorbed on the surface of the catalysts to efficiently catalyze the facile growth of CNTs.<sup>101-104</sup> Most MOFs do not allow *in situ* growth of 1D CNTs as a result of their compositional and structural limitations, and thus, *ex situ* growth strategies have emerged due to the performance advantages exhibited by 1D CNMs. Meanwhile, a 1D hollow structure can generate abundant mesopores, high specific surface area, and a large cavity structure.<sup>105-107</sup> It can also improve the conductivity and stability of the material, and prevent the external environment from corroding the active sites and carbon-coated alloy particles. All in all, the idea of *ex situ* growth of 1D CNTs has been very clear, that is, to use external sources to change the macrostructure of MOF precursors, and to assist metals to catalyze the growth and arrangement of CNTs at high temperatures, which can be expanded into scale-up production for further applications.

**2.2.3. Carbon nanofibers & nanorods.** Except for CNTs, MOF precursors could be thermally transformed into other 1D CNMs, such as carbon nanofibers and nanorods. For example, Smoukov *et al.* pyrolyzed pristine HKUST-1(Cu) polyhedra with (NH<sub>4</sub>)<sub>2</sub>MoS<sub>4</sub> where the intermediate product retains its initial shape, but produces a fibrous nanostructure similar to that in

diatoms on the inside (Fig. 4a).<sup>108</sup> In this case, the combination of Cu and Mo can synergistically promote the formation of fibrous carbons, where most of the Cu NPs condensed on the outside of the carbon matrix, while cooperating with Mo to catalyze the transformation into a fibrous structure (Fig. 4b-e). The unique nano-diatoms arise from a hybrid reaction-diffusion process by combining pyrolysis and metal-based catalysis, as observed in other filamentous carbons by using iron,<sup>109</sup> nickel,<sup>110</sup> and cobalt<sup>111</sup> based catalysts. Different from the nanofiber morphology, Xu *et al.* showed Zn-MOF-74 as the precursor and urea as the regulator to generate the spherical superstructure of MOF nanorods (SS-MOFNR) in Fig. 4f.<sup>112</sup> The formation of SS-MOFNR undergoes a stepwise transition process where 1D MOF nanorods are obtained from the crystallization of dissolved MOF-74 NPs in three directions. They are then carbonized with a well-preserved morphology, in which 1D carbon nanorods are assembled into 3D spherical superstructures (SS-CNRs, Fig. 4g-j). The added urea, cetyltrimethylammonium bromide or polyvinyl pyrrolidone (PVP) are effective regulators to induce structural transformation, which can not only modulate the morphology but also improve the reaction conditions.

In general, by adjusting the original precursors and synthesis conditions, porous MOFs can simultaneously serve as catalysts, carbon sources, templates, and supports for the *in situ* synthesis of 1D carbon nanocomposites *via* thermal transformation.<sup>113,114</sup> Alternatively, their *ex situ* growth can be effectively tuned through additional catalysts and/or carbon sources under certain conditions.<sup>115-117</sup> The pyrolysis of MOF materials helps activate metal-based catalysts and organic components as a result of the energy released by steric confinement effects and the breaking of coordination bonds, and provides favorable conditions for carbon reorganization to form linear 1D carbons.<sup>118</sup> It is not difficult to grow 1D CNTs from MOFs as demonstrated by previous examples, while the facile preparation of 1D carbon nanofibers and nanorods deserve further investigation. Among them, the synthesis of the initial MOF particles is of great significance for the following construction of fine carbon nanostructures. Although a wide variety of 1D carbon nanostructures, including nanotubes, nanofibers, and nanorods, have been synthesized over the past few decades, the fascinating upper layers of anisotropic 1D carbon nanostructures composed of various morphologies as well as structures should be more focused on multifunctional applications.

### 2.3. MOF-derived 2D carbon materials

The “plate” composed of few-layer carbon atoms arranged in a honeycomb network refers to the 2D carbon materials. In the past decade, 2D sp<sup>2</sup>-hybridized CNMs have been widely used in supporting metal species, gas storage, and electrocatalysis thanks to their potentially useful properties.<sup>119-121</sup> To date, graphene nanoribbons can be prepared by oxidation processes, mechanical or chemical exfoliation, plasma etching, top-down organic synthesis, and epitaxial growth.<sup>122-125</sup> Correspondingly, porous planar organic crystalline materials as precursors or templates are also used for the synthesis of 2D nanoribbons.

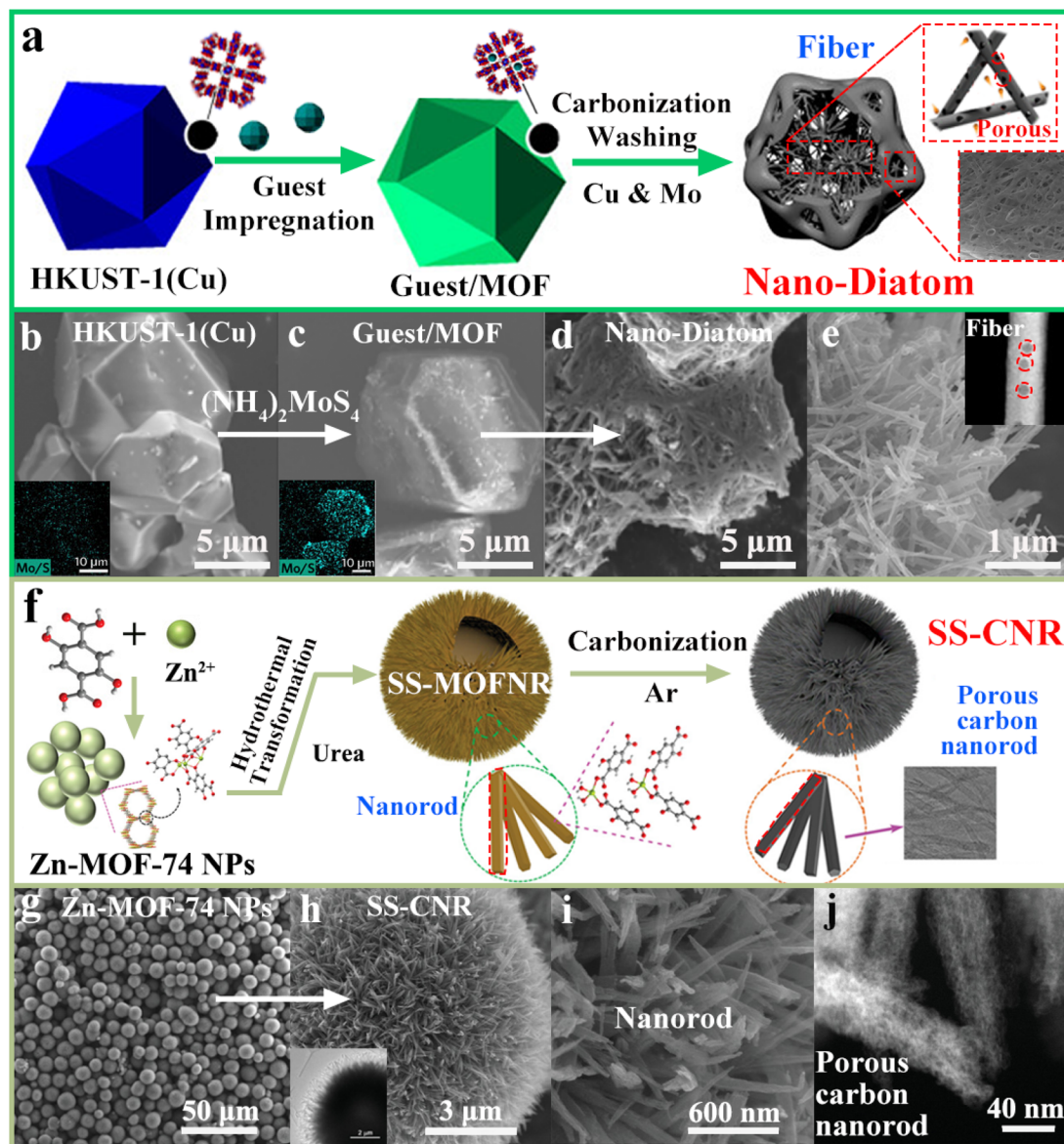


Fig. 4 (a) and (f) Fabrication of MOF-derived 1D nano-diatoms and carbon nanorods, respectively; SEM images of (b) HKUST-1(Cu), (c) guest/MOF, (d) nano-diatoms, and (e) a fiber-like nanostructure ((a)–(e)) reproduced with permission from ref. 108, copyright© 2018, American Chemical Society); (g)–(j) SEM and HAADF-STEM images of Zn-MOF-74, SS-CNR, and carbon nanorods ((f)–(j)) reproduced with permission from ref. 112, copyright© 2019, WILEY-VCH Verlag GmbH & Co. KGaA, Weinheim).

MOFs with different dimensions can be thermally converted into well-defined 2D nanostructures by *in situ* or *ex situ* preparation methods, which is similar to the above-mentioned procedure of synthesizing 1D CNTs. Notably, atomically thin 2D graphene nanoribbons with high aspect ratios show quantum interference effects at the nanoscale resulting in exotic electronic properties, which also offer more possibilities in a wide range of applications.

**2.3.1. Carbon nanoribbons.** Unlike the syntheses of 0D and 1D carbons, the formation of 2D carbon nanoribbons is effectively triggered by the layer-by-layer exfoliation of bulk MOFs.<sup>126,127</sup> On the premise of synthesizing rod-shaped Ni-MOF-rods from nickel nitrate, 1,4-phthalic acid ( $H_2BDC$ ) and 1,4-

diazabicyclo[2.2.2]octane (DABCO), 2D carbon nanoribbon superstructures of graphene nanocages (SGNCs) can be thermally exfoliated (Fig. 5a).<sup>128</sup> As shown in Fig. 5b–e, with increasing temperature, the 3D framework begins to decompose into layered nanostructures, after which the first layer of nanoribbons forms on the surface of the parent MOF. The production of this unique 2D carbon nanolayer is mainly due to the breaking of the metal–N bond on the *z*-axis during MOF pyrolysis, while the metal–O bond in the stronger *x*–*y* plane is retained. With this method, the second layer of carbon nanoribbons continues to grow, starting to transform into 2D carbons. The formed Ni NPs are immobilized in carbon nanocages that play an *in situ* catalytic role in obtaining

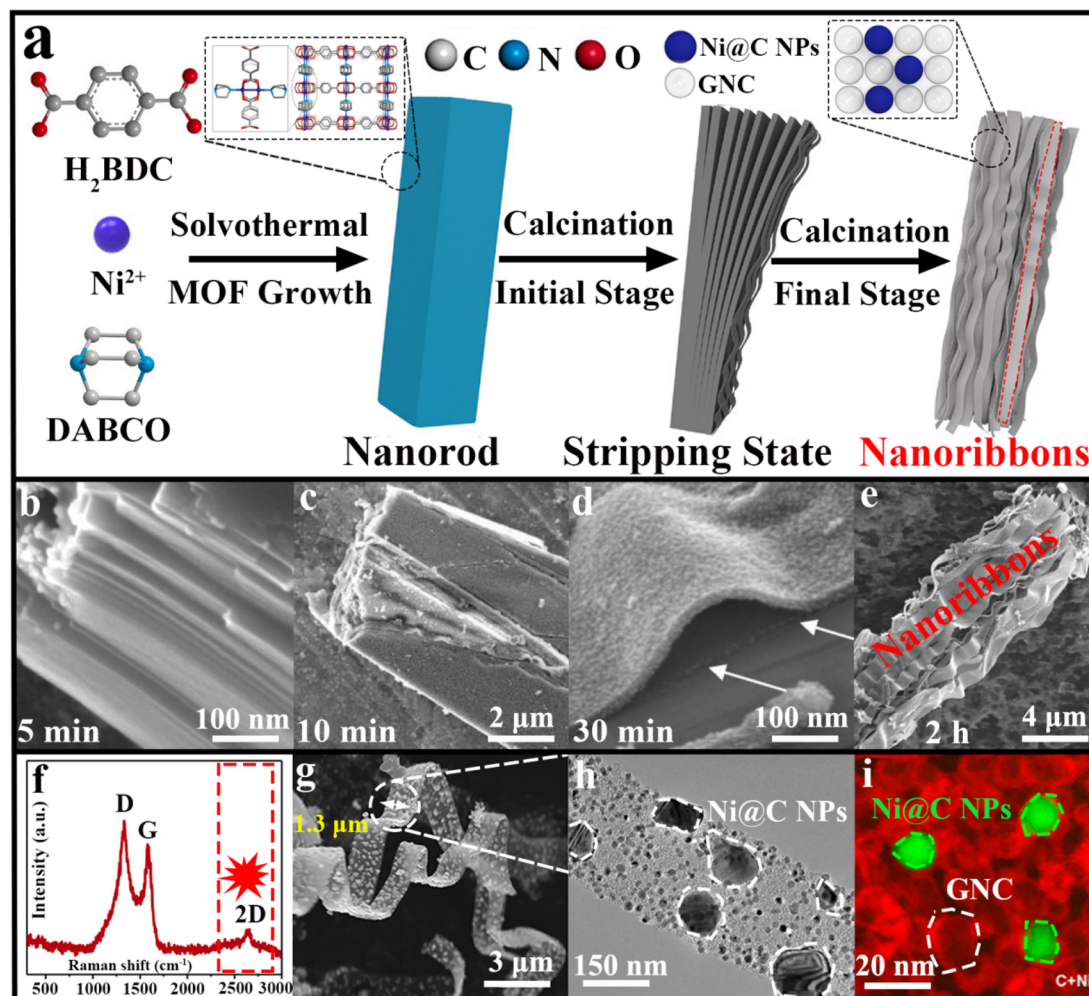


Fig. 5 (a) Schematic preparation of MOF-derived 2D carbon nanoribbons; SEM images of the Ni-MOF nanorod precursor calcined for (b) 5 min, (c) 10 min, (d) 30 min, and (e) 2 h; (f) Raman spectrum; (g)–(i) SEM/TEM image and EELS mapping of SGNC-900 ((a)–(i)) reproduced with permission from ref. 128, copyright© 2020, American Chemical Society).

spherical GNCs with a thickness of 2–3 nm, and finally, in obtaining a bunch of GNCs by layer-by-layer exfoliation. During the high-temperature pyrolysis, highly crystalline graphitic carbon is formed in SGNCs where the tapered ends act as joint support points, and the rectangular nanorods can be transformed into a stack of nanoribbons (Fig. 5f and g). As expected, the molten primary Ni NPs (~10 nm) tend to be agglomerated and generate larger particles of ~100 nm as evidenced by the elemental mapping (Fig. 5h and i). To the best of our knowledge, 2D carbon nanoribbons can be thermally exfoliated from bulk MOFs by simple pyrolysis for the first time, in which no templates and additives are used. In addition, carbon nanoribbons are intricate superstructures composed of interconnected GNCs with large porosity, a high degree of graphitization, and good electrical conductivity that would provide more active sites and facilitate mass transfer for efficient electrocatalysis.

**2.3.2. Graphene nanoribbons and nanomeshes.** As shown in Fig. 6a, the growth of rod-like Zn-based MOF-74 is guided by utilizing a salicylic acid modulator to stabilize Zn(II) sites on the

surface of Zn-MOF crystals.<sup>129</sup> It is observed that the metal Zn species are easily volatilized to result in the formation of uniform carbon nanorods (CNROds) by pyrolysis (Fig. 6b and c). It is further KOH-treated under sonication to give graphene nanoribbons (GNRibs), which exhibit excellent flexibility and few-layer thickness with partially disordered 2D nanosheets, as shown in Fig. 6d. In the meantime, the powder X-ray diffraction (XRD) pattern shows a pair of broad peaks at 25° and 44° corresponding to the (002) and (101) planes of graphitic carbon (Fig. 6e), respectively. On the other hand, Yamauchi *et al.* expanded various ZIF nanocrystals into nanosheets with a 2D crystal structure as well as 2D morphology (Zn-ZIF-L).<sup>130</sup> As a bidentate ligand, 2-methylimidazole (2-MI) presents a zigzag chain unit through the coordination between N atoms and Zn(II) ions (Fig. 6f), which are further integrated by H-bonding to form a supramolecular framework. Inspired by the unique layered structure, the obtained Zn-ZIF-L nanosheets are first selected as precursors instead of conventional ZIFs with 3D structures (Fig. 6g), and exfoliated into ultrathin N-doped graphene nanomeshes (NGMs) using alkali chloride as strippers and

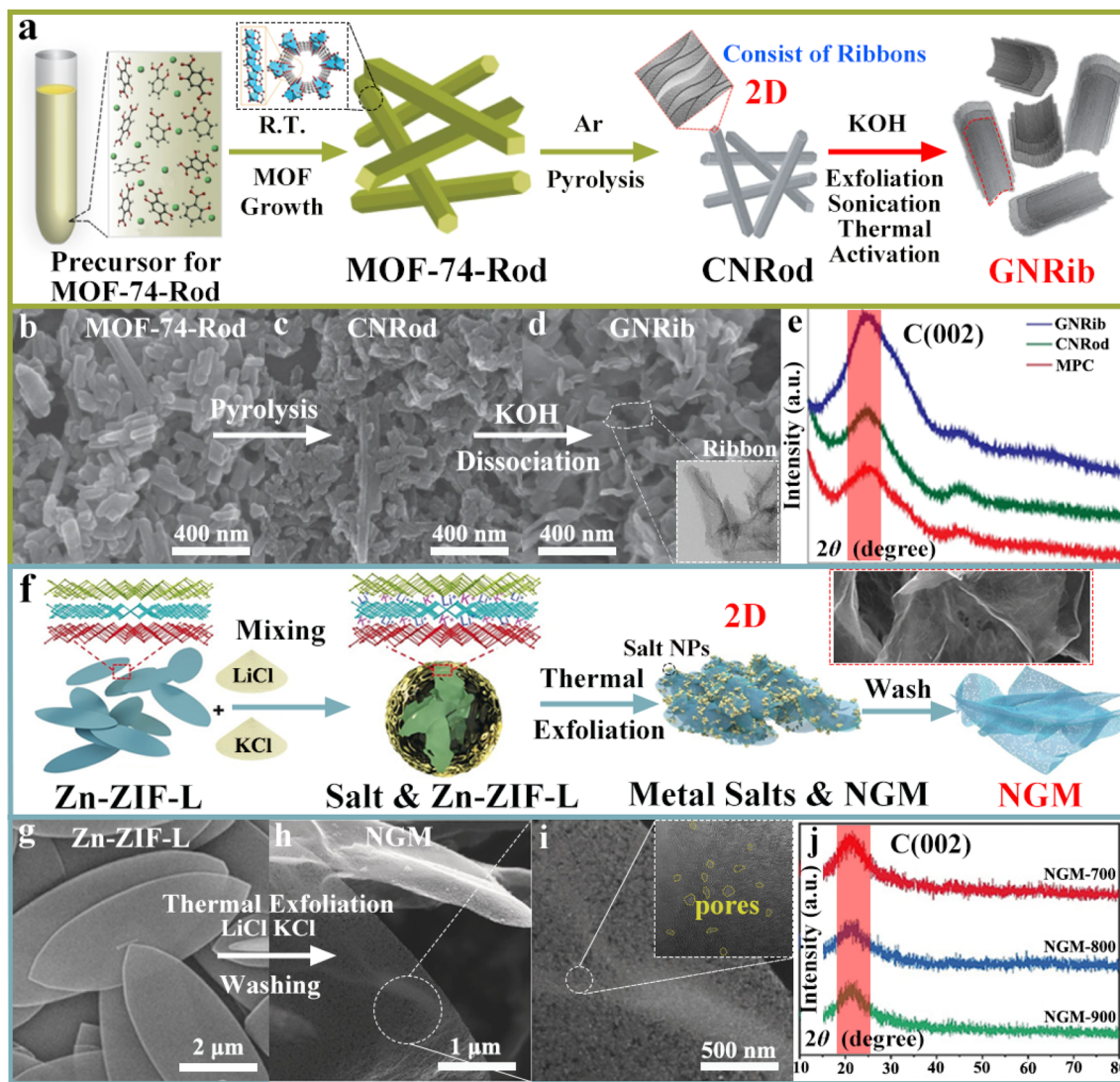


Fig. 6 (a) and (f) Syntheses of MOF-derived 2D GNRib and NGM, respectively; (b) and (d) SEM images of MOF-74-Rod, CNRod and GNRib; (e) XRD curves ((a)–(e)) reproduced with permission from ref. 129, copyright© 2016, Nature Publishing Group); (g)–(i) SEM/TEM images of Zn-ZIF-L and NGM-800; (j) XRD patterns of the NGM-x series ((f)–(j)) reproduced with permission from ref. 130, copyright© 2019, Wiley-VCH Verlag GmbH & Co. KGaA, Weinheim).

etchants. The prepared NGMs have an ultrathin thickness, large specific surface area, high N-doping, and abundant hierarchical pores (Fig. 6h and i). Fig. 6j shows one broad peak at  $\sim 21^\circ$  in the XRD patterns that comes from the diffraction of the (002) plane of low graphitic carbons.

Overall, these above-demonstrated strategies highlight the usefulness of the synthetic approach for the large-scale preparation of high-purity, high-yield 2D *ex situ* grown graphene nanoribbons and nanomeshes using various MOF precursors. These overall structural and compositional advantages of MOF-derived 2D CNMs endow them with satisfactory performance in supercapacitors and metal-ion batteries. In the pyrolytic process, the structures of MOFs change in orientation, and the metal bonds in the Z-axis are easily broken, while the metal bonds in the X-Y plane are still retained, which provides conditions for the self-templating and non-catalytic *in situ*

formation of 2D carbon nanosheets. However, most MOFs still require the addition of regulators or *ex situ* strategies of chemical exfoliation of MOF-derived 3D carbon materials for dimensional reduction to obtain 2D CNMs. It greatly expands 2D CNMs due to their unique ultrathin 2D morphology, high porosity, excellent thermal stability and electrical conductivity, and defective graphene edges. MOF-derived 2D CNMs have multifunctional applications, but their efficient, simple, and mass synthesis strategies also need to be fully realized in the near future.

#### 2.4. MOF-derived 3D carbon materials

To date, most of the reported 3D carbon materials are basically composed of conventional low-dimensional carbon nanostructures (CNTs or graphene) by aggregation or simple self-assembly. In recent years, researchers have more focused on

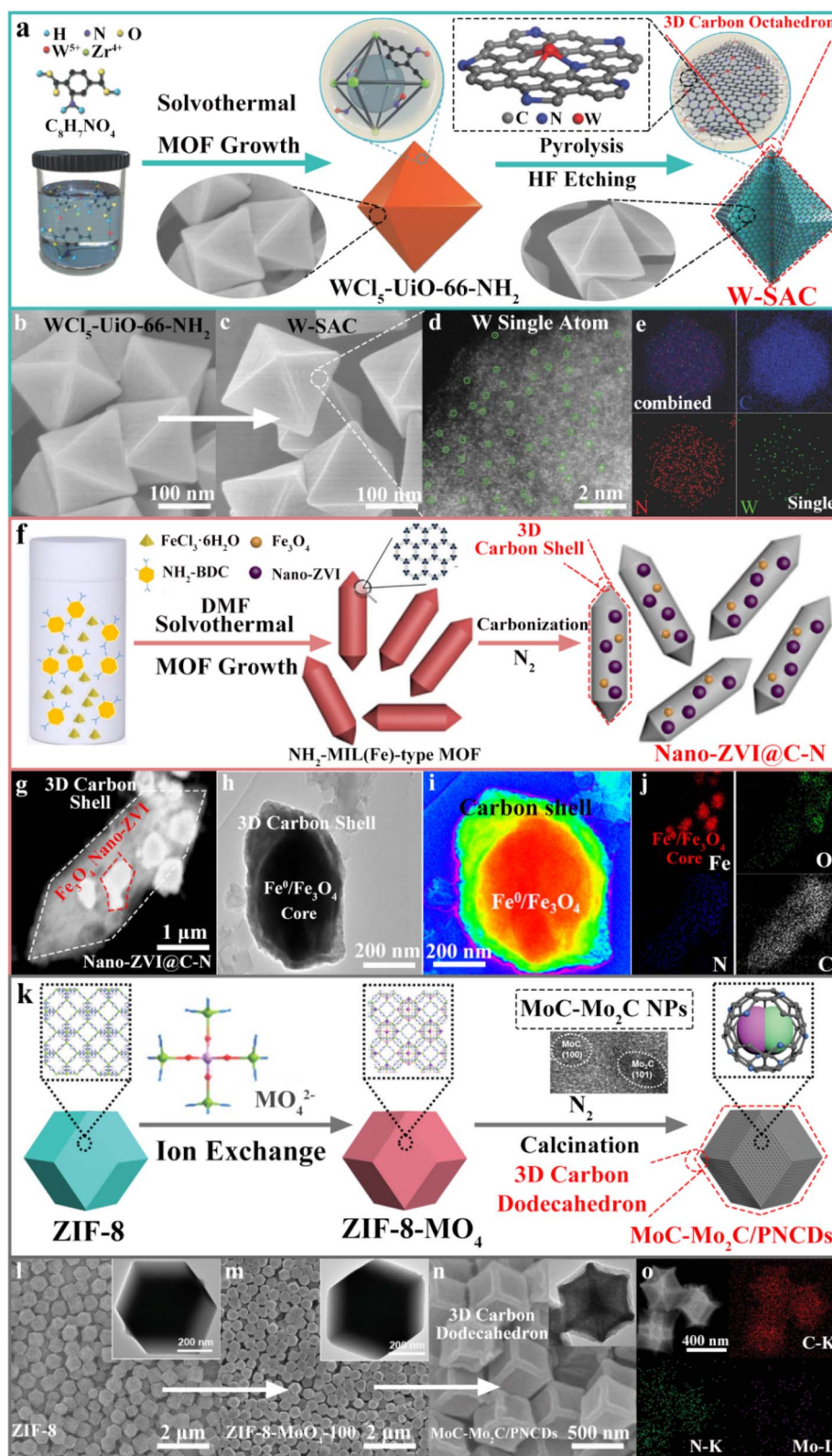


Fig. 7 (a), (f) and (k) Preparation of MOF-derived 3D polyhedral W-SAC, Nano-ZVI@C-N and MoC-Mo<sub>2</sub>C/PNCds, respectively; (b)–(e) SEM/HAADF-STEM images of WCl<sub>5</sub>-UiO-66-NH<sub>2</sub> and W-SAC ((a)–(e)) reproduced with permission from ref. 139, copyright© 2018, WILEY-VCH Verlag GmbH & Co. KGaA, Weinheim); (g)–(j) TEM images and elemental mapping of nano-ZVI@C-N ((f)–(j)) reproduced with permission from ref. 140, copyright© 2020, Elsevier B. V.); SEM images of (l) ZIF-8 and (m) ZIF-8-MoO<sub>4</sub>-100, (n) and (o) SEM images and elemental mapping of MoC-Mo<sub>2</sub>C/PNCds ((k)–(o)) reproduced with permission from ref. 141, copyright© 2019, WILEY-VCH Verlag GmbH & Co. KGaA, Weinheim).

material morphology, density and structure orientation through controlling 3D MOF precursors.<sup>131–133</sup> Thanks to the relatively stable coordination network, carbon materials can well preserve the morphological characteristics of MOFs during the pyrolytic process, providing an ideal framework support for various applications. These obtained 3D porous carbon materials are anticipated to meet the target of “low density and thin thickness” by significantly reducing the density of the material, optimizing reaction intermediates, and promoting the performed reactions.

In this section, we collectively classify and define the unique porous carbons calcined from MOFs as “3D carbon materials”, and the specific surface area, dispersed active sites, and desired mechanical and chemical stability exhibited by such porous nanomaterials are far superior to those of their lower-dimensional counterparts.<sup>134,135</sup> On the other hand, 3D porous carbons are refined by the division of morphology and the synthesis method.<sup>136–138</sup> (1) polyhedral structures obtained by direct pyrolysis of the original MOFs; (2) hollow structures stemming from exogenous etching or internal structure collapse; (3) heterogeneous core-shell structures with a tunable morphological composition; (4) other unique nanostructures such as nanoflowers and multi-level hierarchical morphologies. They all have a common feature of retaining their unique 3D nanostructures from MOF precursors, which also guides the control of the composition and morphology of MOFs to obtain multifunctional MOF-derived 3D CNMs.

**2.4.1. 3D polyhedral carbons.** Currently, the reasonable design and facile preparation of MOF-derived 3D architectures have been developed to maturity compared to other types. For example, Li *et al.* used a pyrolysis strategy to prepare a W-based single-atom catalyst (W-SAC) as shown in Fig. 7a, in which  $\text{WCl}_5$  is first encapsulated into  $\text{NH}_2\text{-UiO-66}$ , and these uncoordinated amine groups prevent the aggregation of W atoms during calcination.<sup>139</sup> After that, the excess zirconia can be efficiently removed by HF etching to give the final product of W-SAC that maintains a polyhedral shape, while W and N are uniformly dispersed within 3D porous N-doped carbon (Fig. 7b–e). Similarly, a spindle-shaped  $\text{NH}_2\text{-MIL(Fe)-88B}$  is first synthesized, and then calcined at high temperature to get a 3D hexagonal rod-shaped Nano-ZVI@C-N, as shown in Fig. 7f.<sup>140</sup> Fig. 7g reveals the presence of core-shell nano-ZVI and  $\text{Fe}_3\text{O}_4$  particles in porous N-doped fusiform carbons. It also shows that Fe atoms are aggregated into spherical NPs of different sizes and embedded in a microporous carbon matrix (Fig. 7h–j). In addition, Lou *et al.* demonstrated the stepwise strategy to obtain  $\text{MoC-Mo}_2\text{C/PNCDS}$  using the single-crystal-to-single-crystal method (Fig. 7k).<sup>141</sup> It is observed that ZIF-8- $\text{MO}_4$  presents smooth corners and a slightly smaller size compared to the initial ZIF-8 dodecahedra due to the occurrence of a partial dissolution/recrystallization process (Fig. 7l and m). Followed by the pyrolysis process, the organic ligands are thermally calcined into 3D porous carbon, which can react with adjacent Mo atoms to form  $\text{Mo}_x\text{C}$  NPs. As expected,  $\text{MoC-Mo}_2\text{C/PNCDS}$  retain a uniform 3D polyhedral morphology with confined ultrafine nanocrystals (Fig. 7n). Finally, the element mapping image confirms an even element distribution of C, N and Mo

(Fig. 7o). In general, the preparation of 3D polyhedral carbons using 3D polyhedral precursors has been regarded as a general, facile, and effective synthetic strategy. Another important aspect of this strategy is the premise that the derived active sites are uniformly distributed over MOF-derived CNMs during high-temperature carbonization. Under these conditions, the obtained catalysts can well inherit the original polyhedral morphology of their precursors, and simultaneously exhibit more stable and superior performance than single low-dimensional structures.

**2.4.2. 3D core-shell carbons.** Compared to typical polyhedral carbons, the 3D core-shell nanostructure is notably featured with abundant interfaces and strong mechanical strength on account of its functional shell and the tunable morphology and composition of the highly active core in the inner space.<sup>142–144</sup> The delicate design of hierarchical 3D core-shell carbons with different layer chemical compositions becomes an effective method to improve their performance. In this context, Sun *et al.* reported the synthesis process of okra-like  $\text{Fe}_7\text{S}_8/\text{C}@/\text{ZnS/N-C}@/\text{C}$  with a core-double shell structure (Fig. 8a).<sup>145</sup> First of all, a uniform MIL-53 template is synthesized and used as the host MOF to combine with the guest ZIF-8, in which the host MIL-53 is modified through the strong affinity of the PVP surfactant. With this method, ZIF-8 particles are self-assembled by electrostatic attraction, thus forming an intriguing MIL@ZIF heterostructure, while resorcinol-formaldehyde (RF) is further *in situ* grown on the surface to improve its structural stability. Finally, after calcination with sulfur, the synthesized MIL@ZIF@RF can be conveniently transformed into core-double shell nanocomposites. Fig. 8b–e confirms the morphological and structural changes of this series of CNMs, and the hierarchical  $\text{Fe}_7\text{S}_8/\text{C}@/\text{ZnS/N-C}@/\text{C}$  nanostructure is well preserved, which can be attributed to the protection of the carbon layer. Meanwhile, the core-shell feature can be verified by the broken part to differentiate the separation between the outer shell and the inner core (Fig. 8f–i). In this case, the stepwise strategy is demonstrated to obtain 3D core-shell carbons from prefabricated MOFs, followed by the pyrolytic procedure. However, the extraordinary core-to-shell transformation mechanism during calcination is worthy of an in-depth study. Furthermore, it should be noted that the structure of 3D CNMs with specific multi-layer shells and heterogeneous cores requires more precise control in synthesis and technology. It would provide the necessary conditions for the facile construction of multifunctional MOF-derived 3D nanomaterials with finely designed structures, and well-defined compositions, morphologies and interfaces.

**2.4.3. 3D hollow carbons.** In addition to conventional 3D polyhedral and core-shell CNMs, these 3D hollow counterparts derived from porous MOFs are also widely reported. In general, the pre-designed hollow MOFs can be conveniently converted into 3D hollow morphology under certain calcination conditions.<sup>146–148</sup> For example, a series of CoM-ZIFs (M = Ni, Mn, Cu, Zn) were self-assembled to synthesize a hollow nanocage (CoM-HNC) through an ion-assisted solvothermal method (Fig. 9a and b).<sup>149</sup> In this case, the internal structure of bimetallic MOF templates evolves into spontaneous hollow intermediates



Fig. 8 (a) Synthesis of 3D core-shell  $\text{Fe}_7\text{S}_8/\text{C}@\text{ZnS}/\text{N}-\text{C}@\text{C}$ ; SEM/TEM images of (b) and (f) MIL-53, (c) and (g) MIL@ZIF, (d) and (h) MIL@ZIF@RF and (e) and (i)  $\text{Fe}_7\text{S}_8/\text{C}@\text{ZnS}/\text{N}-\text{C}@\text{C}$  ((a)–(i)) reproduced with permission from ref. 145, copyright© 2020, WILEY-VCH Verlag GmbH & Co. KGaA, Weinheim).

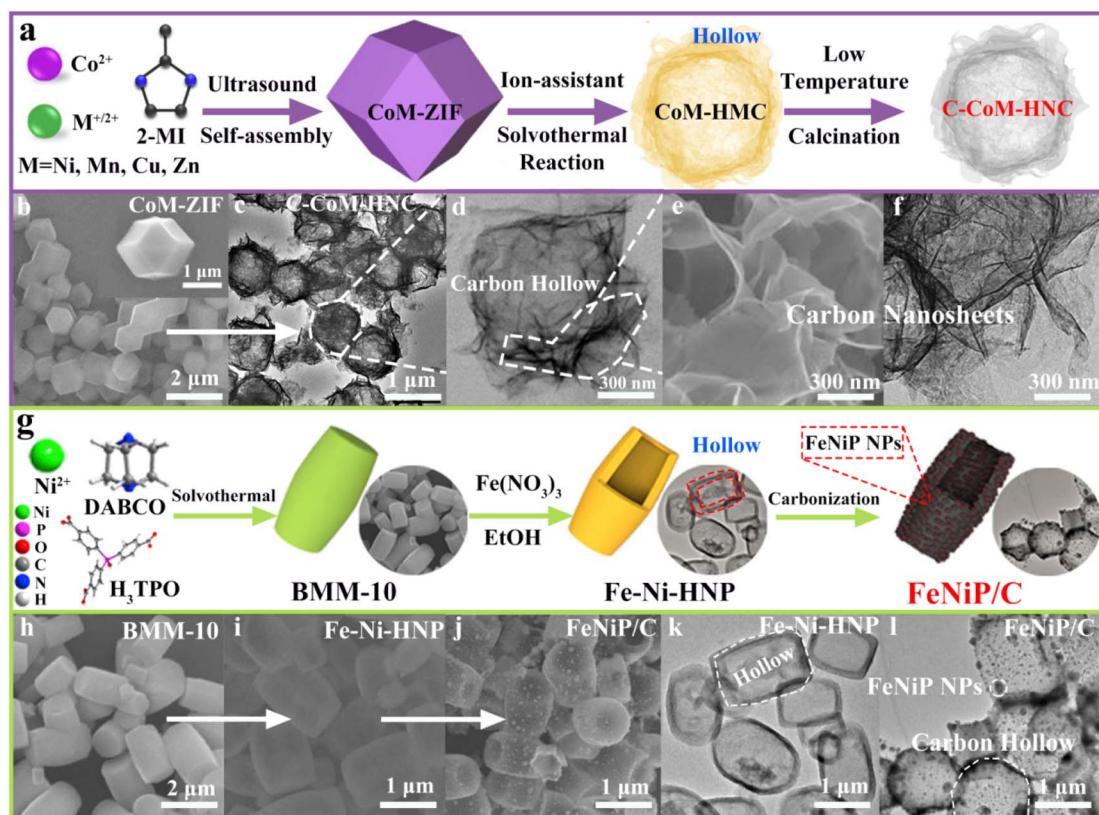


Fig. 9 (a) and (g) Stepwise syntheses of MOF-derived 3D hollow C-CoM-HNC and FeNiP/C; (b)–(f) SEM/TEM images of CoM-ZIF, C-CoM-HNC, and its carbon nanosheets ((a)–(f)) reproduced with permission from ref. 149, copyright© 2020, American Chemical Society); SEM/TEM images of (h) BMM-10, (i) and (k) Fe-Ni-HNP, and (j) and (l) FeNiP/C ((g)–(l)) reproduced with permission from ref. 150, copyright© 2019, Elsevier Ltd).

that are further carbonized into the 3D hollow nanostructure of C-CoM-HNCs with plentiful interlaced carbon nanosheets (Fig. 9c–f). With a similar method, our group previously fabricated a barrel-like microporous MOF of BMM-10, and it would form hollow Fe–Ni–HNPs etched by the hydrolysis of  $\text{Fe}(\text{NO}_3)_3$  (Fig. 9g and h).<sup>150</sup> In this process, it is easy for the outer metal of the MOF to form a relatively stable structure with the coordination of  $\text{H}_2\text{O}$  or  $\text{OH}^-$ , while the flexible ligands in the inner layer are easy to be replaced by protons generated by strong  $\text{Fe}(\text{III})$  hydrolysis. With this method, the outer layer is well retained and the inner layer collapses to form hollow Fe–Ni–HNPs. In Fig. 9i and k, the SEM and TEM images prove that BMM-10 retains the original shape but transforms into a hollow morphology after etching. The carbonization treatment yields one type of 3D hollow bimetallic FeNiP/C where these *in situ* formed FeNiP NPs are firmly anchored onto the carbon layer (Fig. 9j and l). In both cases, such hollow carbon nanostructures are believed to be beneficial for the adequate exposure of active sites and rapid diffusion of reaction substances.

Using a MOF precursor as one type of self-sacrificing template, the internal structure of the crystalline material could be effectively altered by etching and other means under the introduction of foreign metals or etchants. It would avoid the morphology agglomeration and structural collapse of the precursors after calcination. On the other hand, the target product of 3D hollow carbons can be also pyrolyzed directly from single crystals without the tedious treatment to first obtain hollow MOFs, which is novel but challenging.<sup>151–153</sup> Meanwhile, the introduction of heteroatoms into microporous MOFs becomes an effective strategy to adjust the catalytic performance of MOF-derived nanomaterials. This will provide

guidance for the construction of various 3D hollow CNMs from MOF precursors for practical applications.

**2.4.4. Others.** Currently, the strategy of fully highlighting the low-dimensional nanostructures has received extensive attention from the perspective of hierarchical architectures. For example, one type of 3D carbon thorn ball structure based on 2D hard carbon nanosheets has been effectively modulated by using inorganic anions.<sup>154</sup> As shown in Fig. 10a, infinite  $\text{AlO}_4(\text{OH}_2)$  chains are first formed and extended to produce 1D nanosized channels for 2D  $\text{NH}_2\text{-MIL-53(Al)}$ . Then the added sulfate anions react with  $\text{Al}(\text{III})$  ions in the main frame as a result of competitive coordination, resulting in partial substitution of dicarboxylate. After that, the strong aluminum carboxylate bonds are partially decomposed so that the non-layered network tends to be delaminated into a 3D hollow  $\text{NH}_2\text{-MIL-53(Al)}_S$  microsphere (Fig. 10b and c). After pyrolysis, its morphology is well preserved, and abundant 2D S, N, O-rich hard carbon nanosheets (SNO-HCNs) are distributed on the 3D core-shell structure that can significantly shorten the diffusion length of ions, as shown in Fig. 10d–f. Another unique 3D carbon nanoflower structure was successfully synthesized by Xu's group (Fig. 10g).<sup>155</sup> The bimetallic ions coordinate with cyanide and pyridine to form FeNi MOFs using PVP, that is thermally converted into a metal-carbon composite. As shown in Fig. 10h and i, the obtained bimetallic electrocatalyst of FeNi@OCNF inherits the nanoflower morphology with a rough and porous surface, which helps to increase the rapid diffusion of exposed sites and electrolytes. In both cases, the 2D carbon nanostructures could provide more surface as well as near-surface active sites that are conducive to improving the performed catalytic reactions.

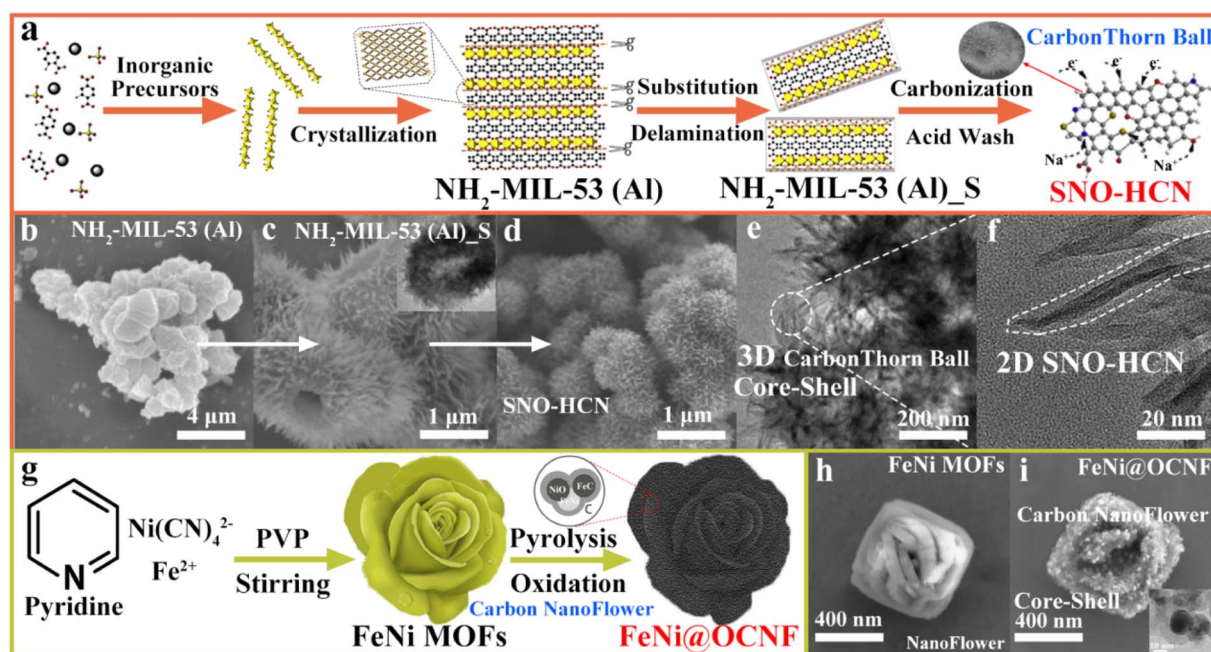


Fig. 10 (a) Chemical delamination of bulk  $\text{NH}_2\text{-MIL-53(Al)}$  into  $\text{NH}_2\text{-MIL-53(Al)}_S$  (reproduced with permission from ref. 154, copyright© 2019, Elsevier B. V.); (b)–(f) SEM/TEM images of MOF precursors and their derivatives; (g) Fabrication of FeNi@OCNF (reproduced with permission from ref. 155, copyright© 2019, Elsevier B. V.); SEM images of (h) FeNi MOFs and (i) FeNi@OCNF.

The complex nanostructure is regarded as a key indicator representing the high catalytic performance of carbon materials. The representative core-shell structures, hollow structures, nanoflowers and hierarchical structures have been widely utilized in electrocatalysis owing to their large specific surface area, uniform active site dispersion, and high mechanical and chemical stability. The introduction of metal species into 3D carbon nanostructures through post-synthesis modification methods to fabricate metal-carbon nanocomposites has also been demonstrated as a feasible strategy to obtain additional host-guest synergistic effects and high catalytic stability. Therefore, these introduced specific synthesis strategies and principles of carbon composites with high-dimensional multi-scale porous structures will provide a desirable reference for the future preparation of multifunctional MOF-derived CNMs.

### 2.5. Self-supported hierarchical structures

Multifunctional MOF structures have been widely developed and demonstrated as self-sacrificial templates for the convenient synthesis of porous nanomaterials with high concentrations of heteroatoms as active metal centers, but the following issues are prone to occur in their synthetic applications: (1) direct contact between various metals produces alloying reactions that induce a negative volume expansion during calcination; (2) some MOFs are limited by their intrinsic nanostructures and are easily sintered, resulting in a great reduction in surface area and active sites; (3) *in situ* formed non-graphitic carbons have low charge transfer, so their contact resistance could be amplified during electrolytic reactions. In addition, the facile preparation of efficient multifunctional MOF-derived materials has become a demand for current application development, which requires innovative design and mass production. To this end, in some recently reported studies, self-supporting conditions are created to introduce materials and assemble NPs into multidimensional nanostructured materials under the condition of the MOF-assisted strategy. With the introduction of self-supporting materials, the versatility of MOF-derived CNMs has been greatly improved, as well as their electrical conductivity, activity and stability for practical applications.

**2.5.1. Self-supported 0D/1D carbons.** In the study of the structure of dissimilar metals, inhibiting their alloying becomes a major problem, while introducing 0D nanomaterials to stabilize their interfacial contacts is regarded as the best choice. In this context, Tang *et al.* chose a ZIF-67 precursor to intercalate 0D Si NPs to obtain Si@ZIF-67 for further thermal treatment (Fig. 11a).<sup>156</sup> In this case, Si@PVP and 2-MI are first uniformly mixed, and then, Co(*n*) ions are added to pre-grow Si/ZIF-67 as shown in Fig. 11b, where Si NPs are successfully encapsulated after *in situ* growth and then carbonized to give Si@c-ZIF (Fig. 11c). From the SEM/TEM images, the Si NPs as hard templates are uniformly distributed to form a dense composite structure, where elemental mapping confirms that Si NPs are completely coated (Fig. 11d-f). In addition, Park *et al.* selected 1D CNTs as self-supporting nanomaterials interwoven with MOFs to form biphasic carbon nanostructures as shown in

Fig. 11g.<sup>88</sup> At first, MOF/CNTs are prepared by directly growing ZIF-8 on 1D CNTs, after which the obtained MOF/CNTs are thermally transformed into porous MOF-C/CNT (Fig. 11h-j). Likewise, the original morphology of ZIF-8 is maintained after carbonization and chemical etching. MOF-C NPs are interwoven and connected with CNTs so that the design combines the inherent properties of MOF-C and CNTs, and fully exploits their respective advantages. Similarly, electrospun 1D polyacrylonitrile (PAN) has also been used to support the growth of bimetallic (BM) ZIFs, which are converted into CNCo-*n*@Fe-*x* series as shown in Fig. 11k and l.<sup>157</sup> In this work, different molar ratios (*n*) of Zn(Ac)<sub>2</sub> and Co(Ac)<sub>2</sub> were electrospun with PAN, and the resulting 1D fibers served as bifunctional templates to provide Zn<sup>2+</sup>/Co<sup>2+</sup> and support the growth of BM ZIFs. Fig. 11m shows a distinct core-shell.

PAN@BMZIF-*n*, and no self-aggregated BMZIF are observed. After etching, the tubular structured BMZIF-*n* is further immersed in Fe-Phen solution to give BMZIF-*n*@Fe-Phen-*x* series, which are further pyrolyzed to obtain CNCo-*n*@Fe-*x* as shown in Fig. 11n-p. The morphology can be well retained, and many tiny 1D multi-walled CNTs are also fabricated owing to the efficient catalysis of metals uniformly distributed in the composites. Therefore, the electrical conductivity can be further improved for these hierarchical MOF-derived CNMs, thereby enhancing their intrinsic electrochemical performance.

**2.5.2. Self-supported 2D/3D carbons.** As discussed previously, both 1D and 2D graphitic carbons, including CNTs and graphene, and 3D carbon architectures can protect active metal sites from acid/base corrosion and provide abundant active sites. Likewise, they are also excellent choices for self-supported substrates of multidimensional CNMs for high-performance reactions. Recently, Wang *et al.* synthesized Ni@N-HCGHF using a combination of hollow-structured Ni-BTC together with 2D graphene oxide (GO, Fig. 12a).<sup>158</sup> After integration, the pre-treated film is further thermally treated with dicyandiamide (DCDA) to generate a layered Ni@N-HCGHF as shown in Fig. 12(b)-(e). Furthermore, the MOF-derived hierarchical superstructure can prevent rGO aggregation, and provide a large surface area and rich active sites, thus significantly enhancing the catalytic performance. On the other hand, 3D supporting substrates or templates have also been extensively used to fabricate MOF-derived CNMs. For example, Co-embedded N-doped CNT (Co@N-CNT) arrays on the 3D self-supported nickel foam (NF) have been successfully synthesized as shown in Fig. 12f.<sup>133</sup> It shows the presence of Co NPs embedded in the CNT arrays, and the layered carbons present hollow nanostructures along the CNT extension direction (Fig. 12g-j). Similarly, 3D inorganic ZnO tetrapods (ZTPs),<sup>159</sup> as well as 3D organic melamine foam (MF),<sup>160</sup> are further utilized as shown in Fig. 12k-o and 12p-t, respectively. In both cases, these MOF-derived metal-carbon nanocomposites in the rigid 3D self-supported substrates exhibit excellent flexibility and mechanical strength, and prevent the collapse of nanostructures. With this method, these structural advantages facilitate electron and electrolyte transport, thereby enhancing the performed electrochemical reactions.

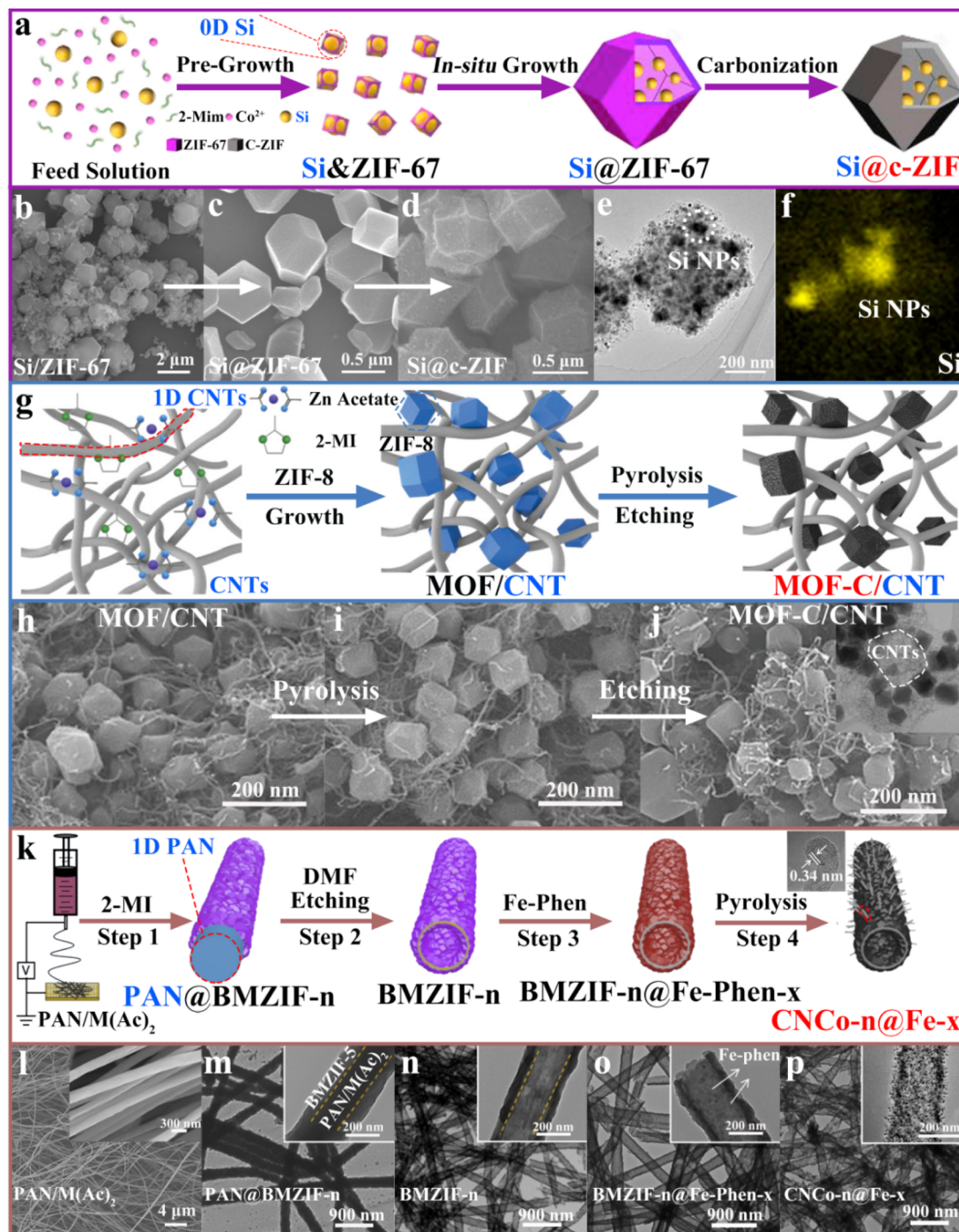


Fig. 11 (a), (g) and (k) Preparation of hierarchical Si@c-ZIF, MOF-C/CNT and the CNCo-*n*@Fe-*x* series; SEM images of (b) Si@ZIF-67, (c) Si@ZIF-67, and (d) Si@c-ZIF; (e)–(f) TEM image and elemental mapping of Si NPs ((a)–(f)) reproduced with permission from ref. 156, copyright© 2020, Elsevier Ltd); SEM images of (h) as-prepared, (i) as-pyrolyzed, and (j) as-etched ZIF-8/CNT ((g)–(j)) reproduced with permission from ref. 88, copyright© 2019, WILEY-VCH Verlag GmbH & Co. KGaA, Weinheim); SEM/TEM images of (l) PAN/M(Ac)<sub>2</sub>, (m) PAN@BMZIF-5, (n) BMZIF-5, (o) BMZIF-5@Fe-Phen-2, and (p) CNCo-5@Fe-2 ((k)–(p)) reproduced with permission from ref. 157, copyright© 2019, Elsevier B. V.).

In general, for these self-supported multidimensional carbon materials, they intrinsically show several structural advantages:<sup>161,162</sup> (i) to provide a good carrier for the orderly growth of MOFs; (ii) to protect the carbon material, and prevent the collapse of the porous frame and particle agglomeration after the carbonization process; (iii) to be flexible so that the

fierce volume change of the attached nanosized carbons under working conditions can be alleviated, which not only ensures the overall stability of the material, but also does not destroy the structure of the carbon material itself; (iv) to ensure stable interfacial connection so that it could provide robust and efficient conduction at the interface for efficient electrocatalysis; (v)

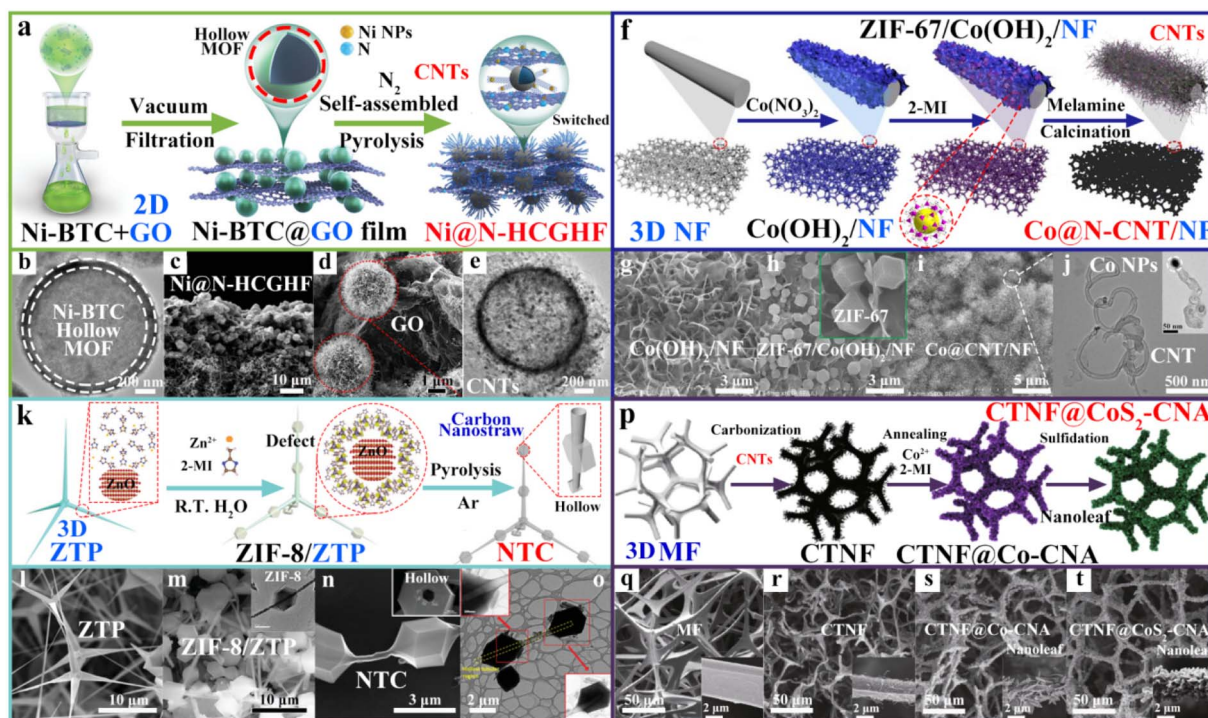


Fig. 12 (a), (f), (k) and (p) Schematic syntheses of hierarchical Ni@N-HCGHF, Co@N-CNT/NF, NTC and CTNF@CoS<sub>2</sub>-CNA; (b) and (e) SEM/TEM images of Ni-BTC-HM and Ni@N-HCGHF ((a)–(e)) reproduced with permission from ref. 158, copyright© 2020, Wiley-VCH GmbH; (g)–(j) SEM/TEM images of Co(OH)<sub>2</sub>/NF and its derivatives ((f)–(j)) reproduced with permission from ref. 158, copyright© 2020, Elsevier B. V.; (l)–(o) SEM/TEM images of ZTP, ZIF-8/ZTP and NTC ((k)–(o)) reproduced with permission from ref. 159, copyright© 2020, WILEY-VCH Verlag GmbH & Co. KGaA, Weinheim); SEM images of (q) MF, (r) CTNF, (s) CTNF@Co-CNA, and (t) CTNF@CoS<sub>2</sub>-CNA ((p)–(t)) reproduced with permission from ref. 160, copyright© 2019, H. Wu et al.).

to be easier to achieve surface hydrophilic/hydrophobic engineering by purposefully adjusting the morphology and microstructure. These novel self-supported nanostructures combined with MOF-derived CNMs open a new way for the design of multidimensional and multifunctional nanomaterials, and can be extended to the preparation of multi-components to show greater application space.

### 3. Applications

Taking the different morphologies of carbon materials calcined from porous MOF precursors as the starting point, we have classified and summarized different types of MOF-derived CNMs, namely 0D, 1D, 2D and 3D. Because of the simplest nanostructure, 0D carbon materials are generally suitable for single electrocatalysis and electromagnetic wave adsorption.<sup>163–166</sup> As the dimensionality of nanomaterials continues to increase, their application fields would be further extended to the research directions of energy, environment and medicine.<sup>167–169</sup> After the birth of 2D and 3D composite structures, multifunctional applications become the most important feature. On account of their large specific surface area and hierarchical pore environment, MOF-derived CNMs have been extensively studied as emerging nanomaterials for diverse research fields. Herein, we have divided their applications into three major fields for a brief introduction and summary, namely, electrocatalysis, energy storage, and environment and sensors.

#### 3.1. Electrocatalysis

As has been discussed above, these MOF-derived CNMs inherit the hierarchically porous nanostructures of their MOF precursors so that they are intrinsically endowed with highly conductive networks. They are featured with well dispersed and uniform active species, large specific surface area, and chemical and physical stability. Therefore, they show great application potential in the field of electrochemical catalysis. The heterogeneous nanostructures of MOF-derived CNMs with different dimensions are extremely special in interface engineering. The physical and chemical properties at the tight interface are completely different from those in the bulk phase, which dictates the multifunctional electrocatalytic properties.<sup>170–174</sup>

Previously, the self-supported 0D/2D heterostructure of NiCoFe-P/C can be well fabricated, which makes the obtained electrocatalyst show excellent hydrogen and oxygen evolution performance (Fig. 13a–c).<sup>175</sup> As a bifunctional catalyst, a low overpotential of 1.55 V for overall water splitting is achieved, which also gives a satisfactory supercapacitor with high performance retention as shown in Fig. 13d–f. Similarly, Chen *et al.* took Zn/Co-ZIF-8 as the “seed” and introduced GO *in situ*. The formed composite shows a 3D structure after pickling and pyrolysis, in which the doped volatilization of Zn and pickling ensure the uniform dispersion of active Co atoms (Fig. 13g).<sup>176</sup> Among them, Co-SAs/N-C/rGO exhibits excellent oxygen reduction thanks to its good cobalt dispersion, abundant accessible

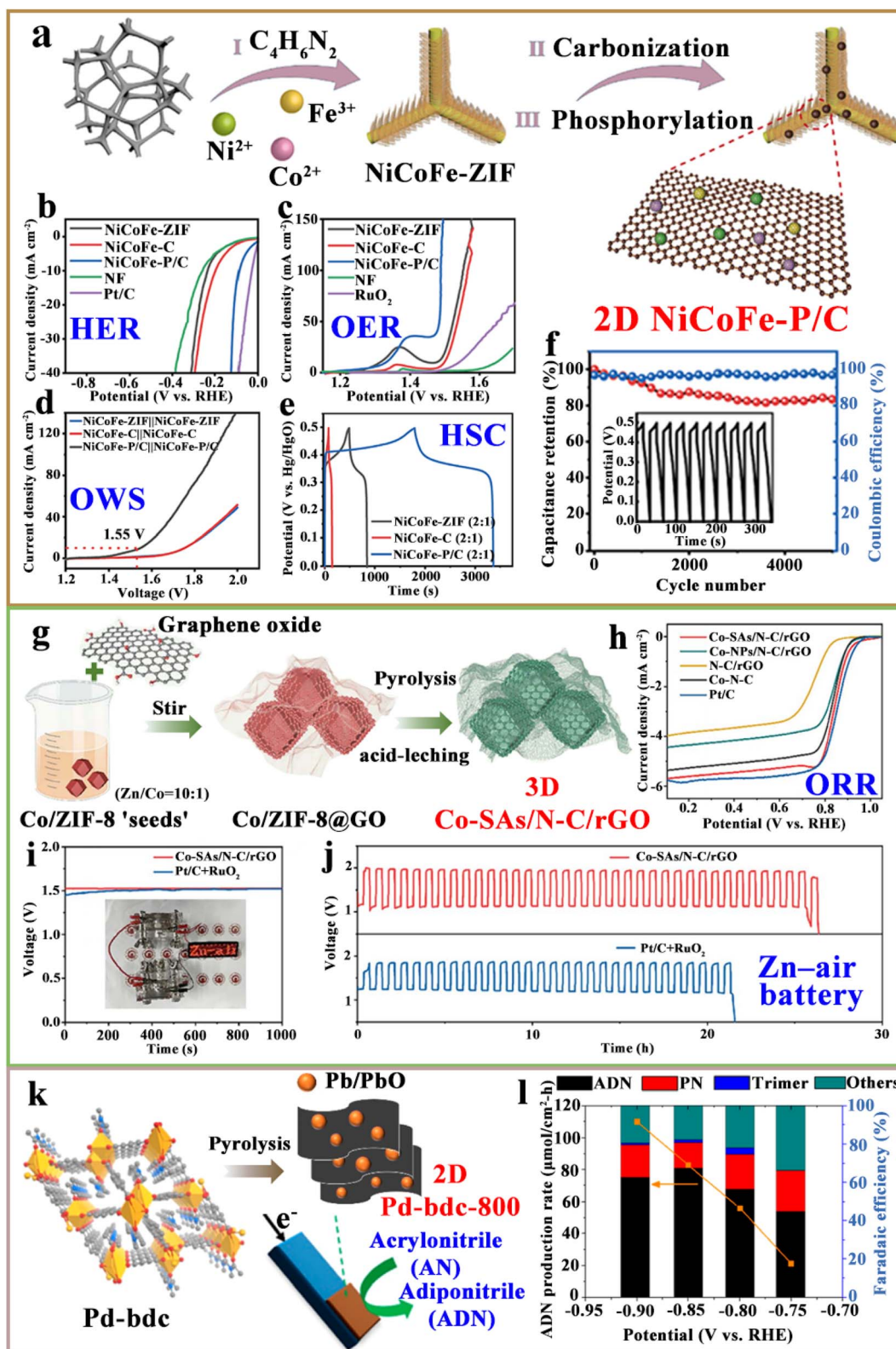


Fig. 13 (a), (g) and (k) Preparation of 2D NiCoFe-P/C, 3D Co-SAs/N-C/rGO and 2D Pd-bdc-800, respectively; (b) and (d) LSV curves of the OER, the HER and OWS; (e)–(f) GCD curves and cycle stability of NiCoFe-P/C ((a)–(f)) reproduced with permission from ref. 175, copyright© 2022, Elsevier B. V. and Science Press; (h)–(i) LSV curves of the ORR and OCV; (j) discharge–charge curve of ZABs ((g)–(j)) reproduced with permission from ref. 176, copyright© 2023, The Royal Society of Chemistry; (l) results of electrolytic experiments conducted at various applied potentials of the Pb-bdc-800-modified electrode ((k) and (l)) reproduced with permission from ref. 177, copyright© 2022, American Chemical Society.

active sites, and improved mass transport as shown in Fig. 13h. Meanwhile, this material can also be applied to assemble Zn–air batteries (ZABs) with excellent stability (Fig. 13i). It has a longer operational time in practical flexible devices than commercial Pt/C + RuO<sub>2</sub> (Fig. 13j). In addition, Kung *et al.* used a Pb-based MOF as a precursor and stripped it into 2D Pd-bdc-800 through pyrolysis (Fig. 13k).<sup>177</sup> The available Pd/PdO composite can efficiently convert acrylonitrile (AN) to adiponitrile (ADN) electrochemically, with an AN reduction efficiency of 67% at a low overpotential. In this case, MOF-derived 2D films have better adhesion to the substrate and show great industrial application space.

In these cases, the rational selection of a suitable substrate, fabrication method, and fine morphology for MOF precursors would lead to fulfillment of the maximum functionality of MOF-derived CNMs. As a result of their diversified and tunable nanostructures, porous MOFs have been regarded as emerging precursors for the facile syntheses of single metal sites or metal compounds (such as oxides, phosphides, sulfides, selenides and others), as well as their composites for electrochemical catalysis.<sup>178–181</sup> On the other hand, compared with other types of MOF derivatives, multifunctional CNMs are structurally endowed with high hydrophobicity due to low polarity caused by the high graphitization degree, which greatly hinders the mass transfer and conduction process of electrocatalytic materials in a liquid. This is a common problem for MOF-derived CNMs, and is also the most urgent problem to be solved at present. Furthermore, the activity and stability of these MOF-derived CNMs with highly dispersed active species are worthy of being studied during the actual electrochemical process, which is crucial for practical applications in catalysis and energy.

### 3.2. Energy storage

In the field of energy batteries, the volume of electrode materials varies greatly during the application of traditional ion batteries, which inevitably causes pulverization of the electrode and overall performance deterioration of batteries. Meanwhile, the low energy density of the devices cannot meet the practical application of electronic devices. On the other hand, the high strength mechanical properties and strain capacity of MOF-derived CNMs can prevent stacked active material particles from extending the electron transport path and blocking ion migration channels. Therefore, it shows broad application prospects for supercapacitors and various batteries in terms of energy storage and conversion.

Semiconductor Si has attracted much attention in the field of lithium-ion batteries (LIBs) due to its superior theoretical capacity and moderate Li-uptake potential. Recently, Yang *et al.* designed some Zn single atoms as the catalyst through the controllable pyrolysis of ZIF-8, and used SiH<sub>4</sub> gas as the silicon source to successfully make the Si-nanodots (NDs) growth through a confined space, and prepared a new silica-based nanomaterial embedded into a MOF-derived nano-reactor as Si-NDs@MDN (Fig. 14a).<sup>182</sup> The prepared full cells with commercial cathode materials show excellent battery

performance, including remarkable cycle stability and high energy density (Fig. 14b and c). By using the same MOF, Fan *et al.* packed one type of small-sized ZIF-8 driven by strong centrifugal force, and then formed a tight structure through the capillary effect induced by methanol evaporation (Fig. 14d).<sup>183</sup> After pyrolysis and acid treatment, a large number of interpenetrating mesoporous pores are conveniently formed between the direct dried porous carbon (DPC), which provides abundant ion transport channels. Because of this, the applications of DPC//DPC symmetrical supercapacitors present high power capability, as well as good cycle performance as shown in Fig. 14e and f. In addition, when applied to potassium ion batteries (PIBs), one kind of 3D Ni-doped FeSe<sub>2</sub>/Fe<sub>3</sub>Se<sub>4</sub> encapsulated by Se-doped carbon (NF<sub>11</sub>S/C) is used to assemble the PIB cells to present considerable rate performance, whose reversible capacity is tested by 1200 cycles to verify its cycle stability (Fig. 14g).<sup>184</sup> As shown in Fig. 14h and i, the excellent electrochemical performance of the whole cell further proves the practical application potential of MOF-derived CNMs in PIBs.

Due to the strong carbon network structure, MOF-derived CNMs exhibit much better stability than other derivatives. Using low boiling point components to construct ordered interpenetrating structures has become a new direction of combining MOF materials with battery energy in the future.<sup>185–188</sup> In addition to the above structural components, the exploitation of multifunctional and cost-efficient non-noble-metal based carbon catalysts is endowed with practical significance for energy conversion and storage. However, there is still a problem that cannot be ignored. Compared with the other derivatives, graphitic carbons in CNMs are thermodynamically unstable under the action of internal metal ions during calcination, which would lead to the deterioration of application performance. How to deal with the structure–activity relationship between metal and graphitic carbon remains a significant issue in the field of energy.

### 3.3. Environmental and sensors

In addition to catalysis and energy, these multifunctional MOF-derived CNMs play an equally important role in the field of environmental detection and sensing.<sup>189–191</sup> This series of nanocomposites are not only an effective probe to detect the concentration of hazardous ions in the environment, but can also be developed as an efficient catalyst to absorb and degrade harmful substances. In this context, Caruso *et al.* obtained a self-supported carbon composite by inserting carbon dots into Au/Uio-66, and then obtained HS-C/Au/Uio-66 through thiolation (Fig. 15a).<sup>192</sup> The surface plasmon resonance of the metal NPs combines with the fluorescence signal where the film of its powder shows a significant change in fluorescence intensity, which is used to selectively detect the Pb(II) ions as shown in Fig. 15b. Secondly, Yin's team used porous carbon (PC) as a substrate, first introduced ZIF-8, and then grew secondary ZIF-67, and prepared the final product of 3D Co@CNT/PC-920 through carbonization (Fig. 15c).<sup>193</sup> When the matching thickness equals 2.30 mm, the minimum

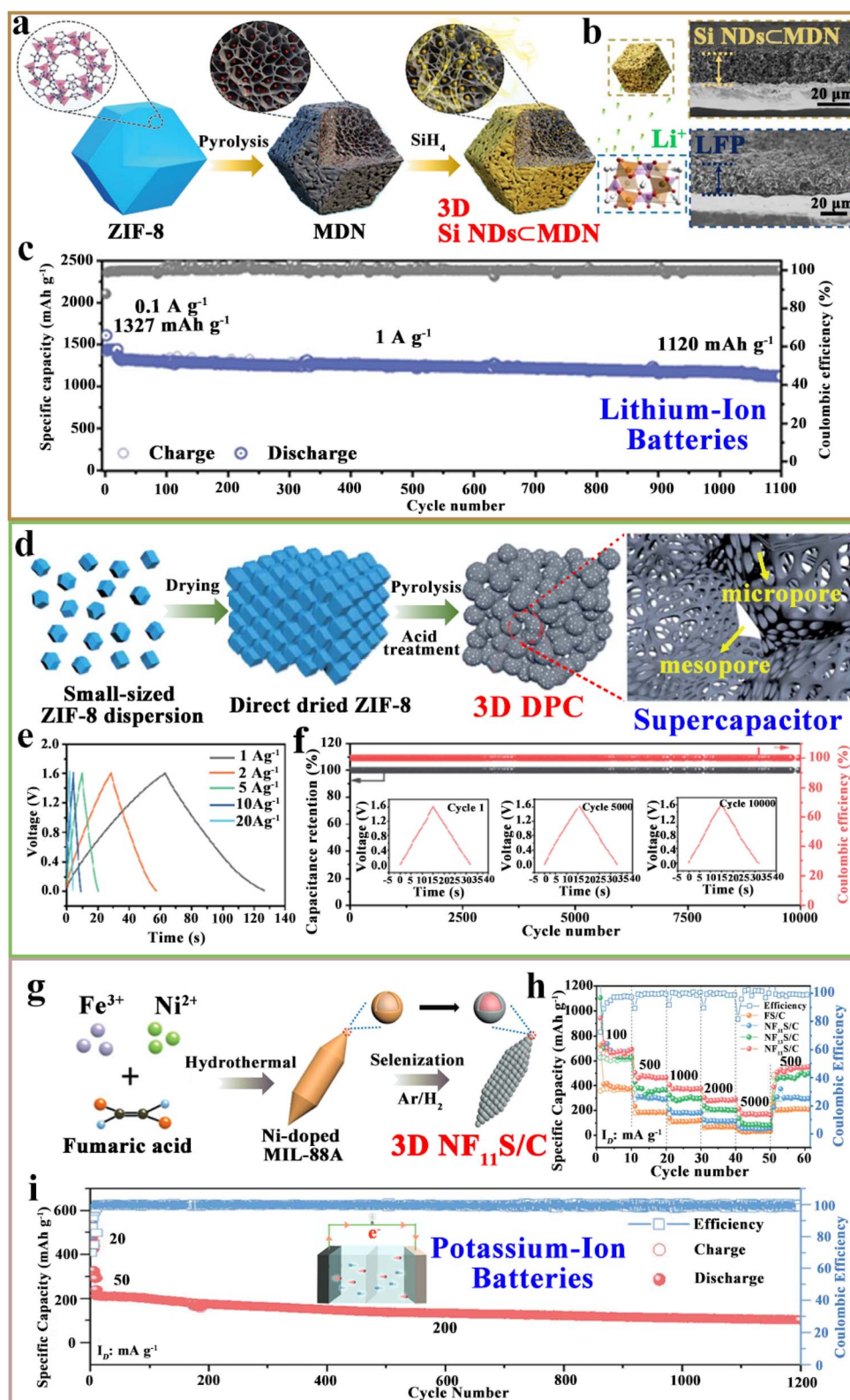


Fig. 14 (a), (d) and (g) Preparation of 3D Si NDs@MDN, 3D DPC and 3D NF<sub>11</sub>S/C, respectively; (b) electrode configuration of the Si ND based full cells; (c) cycling performance of the Si NDs@MDN framework electrode ((a)–(c)) reproduced with permission from ref. 182, copyright© 2022, Wiley-VCH GmbH); (e) and (f) GCD curves and cycling stability performance of DPC//DPC symmetric supercapacitors ((d)–(f)) reproduced with permission from ref. 183, copyright© 2022, The Royal Society of Chemistry); (h)–(i) rate performance and cycling stability of NF<sub>11</sub>S/C electrodes, respectively ((g)–(i)) reproduced with permission from ref. 184, copyright© 2022, Wiley-VCH GmbH).

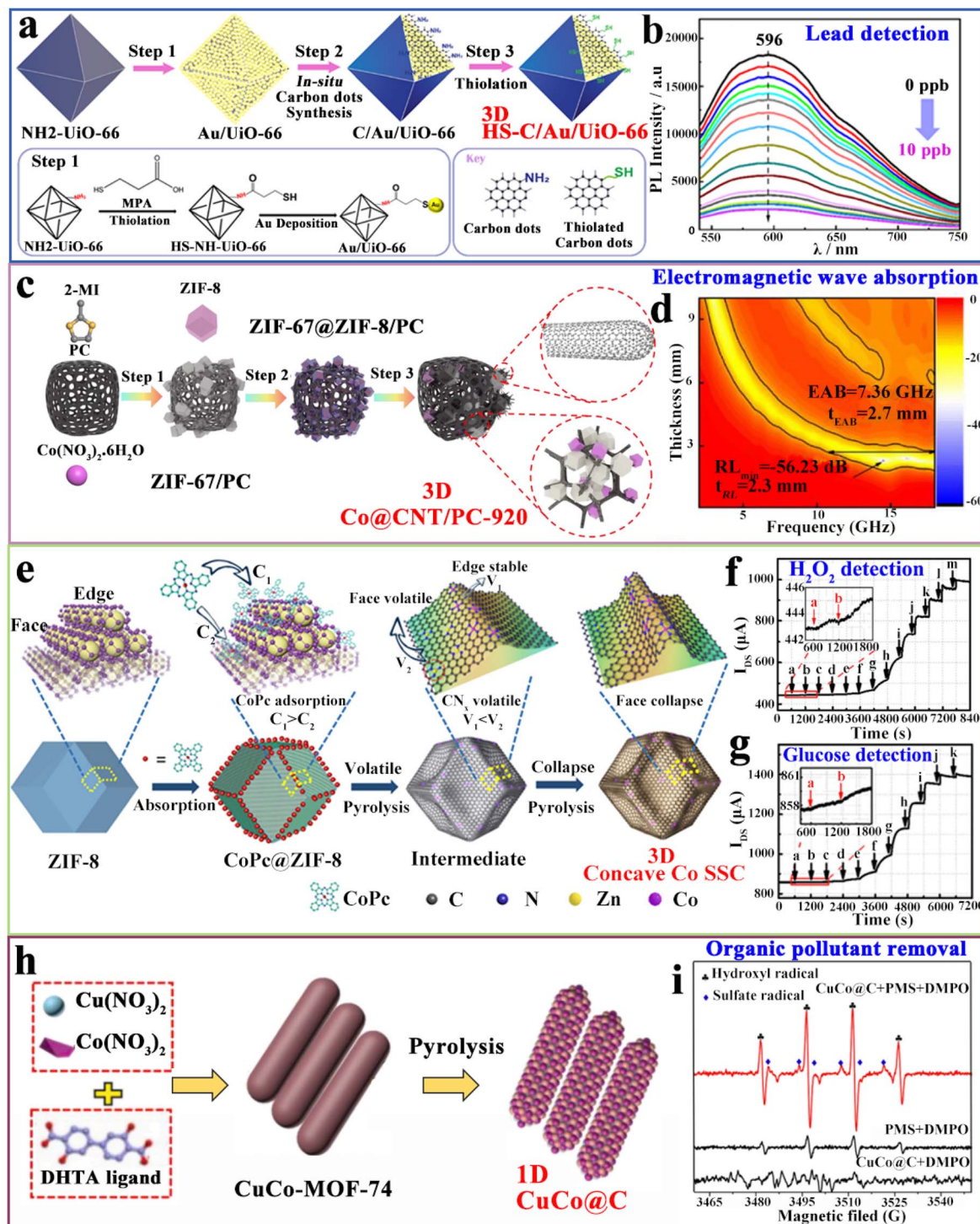


Fig. 15 (a), (c), (e) and (h) Schematic diagrams for the facile fabrication of 3D HS-C/Au(x)/UiO-66, 3D Co@CNT/PC-920, 3D Co SSC and 1D CuCo@C, respectively; (b) fluorescence emission spectra of HS-C/Au(1.4)/UiO-66 films ((a) and (b)) reproduced with permission from ref. 192, copyright© 2022, American Chemical Society); (d) the 2D color map of Co@CNT/PC-920 ((c) and (d)) reproduced with permission from ref. 193, copyright© 2022, Elsevier B. V.); (f) and (g) channel current response for H<sub>2</sub>O<sub>2</sub> and glucose ((e)–(g)) reproduced with permission from ref. 194, copyright© 2022, Elsevier B. V. and Science China Press); (i) effect of radical scavengers on OG removal ((h) and (i)) reproduced with permission from ref. 195, copyright© 2022, Elsevier B. V.).

reflection loss (RL) is  $-56.23$  dB, and its effective absorption bandwidth (EAB) reaches 7.36 GHz as shown in Fig. 15d. Thirdly, Yu *et al.* demonstrated a ZIF-8 dodecahedron as an

ideal matrix to host Co(II) phthalocyanine (CoPc) molecules, where the anisotropic heat evaporation rate allows the edge frame to be maintained during pyrolysis, while the planar

surface is collapsed to form the concave Co single site catalyst (Co SSC, Fig. 15e).<sup>194</sup> In terms of detection sensing, the Co SSC modified SGGT channel current response is much larger than that of bare Au for H<sub>2</sub>O<sub>2</sub>, while the as-prepared glucose sensor combined with the enzyme catalyst also gives an excellent catalytic activity, as shown in Fig. 15f and g. Furthermore, Tang's group fabricated 1D CuCo carbon nanorods (CuCo@C) by direct carbonization of bimetallic rod-shaped CuCo-MOF-74 as shown in Fig. 15h.<sup>195</sup> From the competitive quenching experiments, it is observed that the signal intensity of DMPO-<sup>\*</sup>OH increases sharply using CuCo@C (Fig. 15i), proving the possibility of effectively degrading Orange G in a wide range of pH values.

These examples make it possible to develop hierarchical MOF-derived CNMs as suitable absorbing materials or highly sensitive sensors to resolve environmental issues. In the meantime, the formation of CNTs or the addition of guest active species into these carbon materials would enhance the heterogeneous interface, increase catalytic centers as well as improve conductive pathways for efficient environmental biosensors and healthcare applications. Currently, MOF-derived defective carbons have emerged as one of the most promising electrocatalysts to substitute noble-metal based ones as a result of their intrinsic advantages, including environmental friendliness, cost-effective and high structural tunability. Though theoretical results have clearly shown the importance and effectiveness of carbon defects in catalysis, energy, environmental protection and sensors, it remains a huge challenge to experimentally demonstrate these ideas. Furthermore, it is also an extremely tough task to precisely characterize and accurately distinguish MOF-derived defective CNMs under the real working conditions.

## 4. Conclusions and perspectives

In conclusion, this review highlights the recent progress on MOF-derived multidimensional CNMs for multifunctional applications in the last five to ten years. Various synthetic methods for the facile and controllable preparation of MOF-derived CNMs with different dimensions are fully discussed, and their formation principles and mechanisms are also analyzed in detail. Finally, we have also introduced their multifunctional applications in two main fields of energy catalysis and environmental detection. Under these circumstances, we believe that the fabrication of versatile MOFs and their carbon-based derivatives remains a hot research topic, which will receive more and more research interest in the near future.

Although a series of MOF-derived CNMs have been synthesized and applied in many research applications, the systematic preparation of MOF-derived multidimensional CNMs is still in its infancy, and more efforts are needed. Below are some unexplored but foreseeable key issues that should be carefully considered:

(1) Synthetic method: from MOF precursors to their final products of multidimensional CNMs, the precise control of their morphologies and surface chemistry remains a major

challenge in the advanced synthetic methods for the facile syntheses of MOF-derived CNMs.

(2) Pyrolytic mechanism: our discussion mainly focuses on some common MOFs, such as the ZIF series, MIL series, PBA series, HKUST-1, *etc.*, but usually ignores the sintering phenomenon that occurs in almost all MOFs during carbonization. Therefore, it is of great significance to obtain new MOFs and their carbon-based derivatives where the formation principles and mechanisms are elaborately worked out.

(3) Advanced characterization: *in situ* characterization of the growth mode and morphology of multidimensional CNMs under the real synthetic conditions needs to be further improved. Despite the rapid development of techniques for the characterization of nanomaterials at the nanoscale, monitoring of their growth mode during synthesis is far from satisfactory, which is particularly important for theoretical research and morphology regulation.

(4) Mass production: the reaction conditions required to obtain the target CNMs are normally harsh, and the limitations of the preparation time, temperature, reaction instruments, and synthesis steps are still completely restricted to the laboratory production level, and most of them still rely on CVD technology. On the other hand, for MOF-derived multidimensional CNMs with excellent properties, the synthesis efficiency is still far lower than that of other industrialized commercial chemicals. The road to industrialization is still long, and overly complex synthetic steps still require a clear mechanism for cost simplification.

(5) Application limitation: for practical applications, the high hydrophobicity of CNMs has a great influence on the mass transfer in the catalytic process. Similarly, carbon materials are thermodynamically unstable due to the action of internal metal ions, resulting in reduced battery performance. Proper doping of heterogeneous elements can effectively improve this situation, which deserves to be further proved by a large number of experiments. It is still a key issue to break through the application limitations of carbon-based materials from MOF precursors.

The field of MOF-derived multidimensional CNMs is facing considerable development as well as huge challenges. In the future, more research is needed to combine the stability of the regular structure of MOFs with the advantages of versatile carbon materials, so as to design and discover more new functional nanomaterials or nanocomposites. It is anticipated to explore the commonality and difference in the morphology dimension, synthesis method and principle mechanism to achieve more efficient industrial preparation, more clear theoretical mechanism guidance and broader application space. Finally, this review will provide new insights into the rational design and facile synthesis of multifunctional MOF-derived CNMs with targeted nanostructures, tunable compositions, and rich functionalities, thereby exhibiting extremely high prospects in these energy and environment applications.

## Abbreviations

0/1/2/3D	0/1/2/3-Dimension
2-MI	2-Methylimidazole

Ac	Acetate	NCNHP	N-doped carbon nanotube hollow polyhedron
ADN	Adiponitrile	NDs	Nanodots
AN	Acrylonitrile	NF	Nickel foam or nanoflower
BDC	1,4-Benzenedicarboxylic acid	NGMs	N-doped graphene nanomeshes
BM	Bimetallic	NMC	N-doped mesoporous carbons
BMM-10Bimetallic	of the MOF [Ni <sub>2</sub> (TPO) <sub>4/3</sub> (dabco)]·guest	N-PCL	N-doped porous carbon leave
CGHF	CNT/reduced graphene oxide heterostructure film	NPs	Nanoparticles
CNHO	CNT-assembled hierarchical porous octahedron	OCV	Open-circuit voltage
CNA	Carbon nanoleaf array	OER	Oxygen evolution reaction
CNMs	Carbon nanomaterials	OG	Orange G
CNRs/	Carbon nanorods	OLCS	Onion-like carbon sphere
CNRods		ORR	Oxygen reduction reaction
CNTs	Carbon nanotubes	OVS	Overall water splitting
CTNF	CNT-wrapped N-doped carbon foam	PAN	Polyacrylonitrile
CVD	Chemical vapor decomposition	PB	Prussian blue
DABCO	1,4-Diazabicyclo[2.2.2]octane	PBA	Prussian blue analogue
DCDA	Dicyandiamide	PCL	Porous carbon leaves
DHTA	2,5-Dihydroxyterephthalic acid	Phen	1,10-Phenanthroline
DMF	<i>N,N</i> -Dimethylformamide	PIB	Potassium ion battery
DMPO	5,5-Dimethyl-1-pyrroline N-oxide ( <a href="https://www.chembk.com/en/chem/5,5-dimethyl-1-pyrrolineN-oxide">https://www.chembk.com/en/chem/5,5-dimethyl-1-pyrrolineN-oxide</a> )	PN	Propionitrile
DPC	Direct porous carbon	PNCDS	Porous nitrogen-doped carbon dodecahedra
EAB	Effective absorption bandwidth	PVP	Polyvinyl pyrrolidone
FSZABFlexible	solid-state Zn-air battery	RF	Resorcinol-formaldehyde
GCD	Galvanostatic charge/discharge	rGO	Reduced graphene oxide
GNCs	Graphene nanocages	RL	Reflection loss
GNRibs	Graphene nanoribbons	RT	Room temperature
GO/rGO	Graphene oxide/reduced graphene oxide	SAC	Single-atom catalyst
H <sub>2</sub> BDC	1,4-Phthalic acid	SAs	Single atom sites
HAADF-STEM	High-angle annular dark field scanning TEM	SEM	Scanning electron microscope
HCGHF	Hollow-microsphere CNT/reduced graphene oxide heterostructure film	SGGT	Solution gated graphene transistor
HF	Hydrofluoric acid	SGNCs	Superstructures of graphene nanocages
HKUST	The Hong Kong University of Science and Technology	SNO-HCNs	S, N, O-rich hard carbon nanosheets
HNCs	Hollow nanocages	SS	Spherical superstructure
HNPs	Hollow nanoparticles	SSC	Single site catalyst
HOMO	Highest occupied molecular orbital	TEDA	Triethylenediamine
HPCNs	Hollow porous carbon nanofibers	TEM	Transmission electron microscope
HRTEM	High-resolution transmission electron microscope	UiO	University of Oslo
HSC	Hybrid supercapacitor	XRD	X-ray diffraction
LIB	Lithium-ion battery	ZIF	Zeolite imidazole framework
LSB	Lithium-sulfur battery	ZTPs	ZnO tetrapods
LSV	Linear sweep voltammetry	ZVI	Zero-valent ion
LZAB	Liquid Zn-air battery		
MDN	Metal organic framework-derived nanoreactor		
MeOH	Methanol		
MF	Melamine foam		
MIL	Material institute Lavoisier		
MOFs	Metal-organic frameworks		
MOFNR	Metal-organic framework nanorod		
MPA	3-Mercaptopropionic acid		
MSHMs	Multi-shelled hollow microspheres		
NC	N-doped carbon		

## Author contributions

The manuscript was written through the contributions of all authors. All authors have given approval to the final version of the manuscript.

## Conflicts of interest

The authors declare no competing financial interest.

## Acknowledgements

This work was financially supported by the National Natural Science Foundation of China (21601137), the Basic Science and Technology Research Project of Wenzhou, Zhejiang Province

(H20220001), and the Special Basic Cooperative Research Programs of Yunnan Provincial Undergraduate Universities Association (202101BA070001-042).

## References

- S. Ali Akbar Razavi and A. Morsali, *Coord. Chem. Rev.*, 2019, **399**, 213023.
- L. Zhong, J. Ding, J. Qian and M. Hong, *Coord. Chem. Rev.*, 2021, **434**, 213804.
- Y. Deng, Y. Wu, G. Chen, X. Zheng, M. Dai and C. Peng, *Chem. Eng. J.*, 2021, **405**, 127004.
- V. Richards, *Nat. Rev. Chem.*, 2017, **1**, 0018.
- Y.-S. Li, H. Bux, A. Feldhoff, G.-L. Li, W.-S. Yang and J. Caro, *Adv. Mater.*, 2010, **22**, 3322–3326.
- X. Liu, B. Qian, D. Zhang, M. Yu, Z. Chang and X. Bu, *Coord. Chem. Rev.*, 2023, **476**, 214921.
- A. Taroni, *Nat. Mater.*, 2013, **12**, 688.
- M. Kim, R. Xin, J. Earnshaw, J. Tang, J. P. Hill, A. Ashok, A. K. Nanjundan, J. Kim, C. Young, Y. Sugahara, J. Na and Y. Yamauchi, *Nat. Protoc.*, 2022, **17**, 2990–3027.
- Y. Shi, B. Zhu, X. Guo, W. Li, W. Ma, X. Wu and H. Pang, *Energy Storage Mater.*, 2022, **51**, 840–872.
- C. Wang, J. Kim, J. Tang, M. Kim, H. Lim, V. Malgras, J. You, Q. Xu, J. Li and Y. Yamauchi, *Chem*, 2020, **6**, 19–40.
- J. Xu, Y. Xu and X.-H. Bu, *Small*, 2021, **17**, 2102331.
- S. Jin, *ACS Energy Lett.*, 2019, **4**, 1443–1445.
- X. Ming, A. Wei, Y. Liu, L. Peng, P. Li, J. Wang, S. Liu, W. Fang, Z. Wang, H. Peng, J. Lin, H. Huang, Z. Han, S. Luo, M. Cao, B. Wang, Z. Liu, F. Guo, Z. Xu and C. Gao, *Adv. Mater.*, 2022, **34**, 2201867.
- W. Tian, H. Zhang, Z. Qian, T. Ouyang, H. Sun, J. Qin, M. O. Tadé and S. Wang, *Appl. Catal., B*, 2018, **225**, 76–83.
- J. Xu and M. Antonietti, *J. Am. Chem. Soc.*, 2017, **139**, 6026–6029.
- Y. Dong, Q. Wang, H. Wu, Y. Chen, C.-H. Lu, Y. Chi and H.-H. Yang, *Small*, 2016, **12**, 5376–5393.
- R. R. Salunkhe, Y. V. Kaneti, J. Kim, J. H. Kim and Y. Yamauchi, *Acc. Chem. Res.*, 2016, **49**, 2796–2806.
- F. Xue, X. Qi, T. Huang, C. Tang, N. Zhang and Y. Wang, *Chem. Eng. J.*, 2021, **419**, 129620.
- Z. Li, L. Deng, I. A. Kinloch and R. J. Young, *Prog. Mater. Sci.*, 2023, 101089.
- Y. Tang, J. Ding, W. Zhou, S. Cao, F. Yang, Y. Sun, S. Zhang, H. Xue and H. Pang, *Adv. Sci.*, 2023, 2206960.
- Y. Wang, M. Zhang, X. Shen, H. Wang, H. Wang, K. Xia, Z. Yin and Y. Zhang, *Small*, 2021, **17**, 2008079.
- J. Lee, J. Kim and T. Hyeon, *Adv. Mater.*, 2006, **18**, 2073–2094.
- W. Liu, F. Zhu, B. Ge, L. Sun, Y. Liu and W. Shi, *Chem. Eng. J.*, 2022, **427**, 130788.
- F. Liu, S. Liu, J. Meng, F. Xia, Z. Xiao, Z. Liu, Q. Li, J. Wu and L. Mai, *Nano Energy*, 2020, **73**, 104758.
- L. Yang, X. Zeng, W. Wang and D. Cao, *Adv. Funct. Mater.*, 2018, **28**, 1704537.
- H. Zou, X. Li, W. Zheng and X. Zhou, *Biochem. Biophys. Res. Commun.*, 2022, **608**, 116–121.
- V. K. Abdelkader-Fernández, D. M. Fernandes and C. Freire, *J. CO<sub>2</sub> Util.*, 2020, **42**, 101350.
- C. Zhu and H. Xia, *Acc. Chem. Res.*, 2018, **51**, 1691–1700.
- R. Freund, O. Zaremba, G. Arnauts, R. Ameloot, G. Skorupskii, M. Dincă, A. Bavykina, J. Gascon, A. Ejsmont, J. Goscianska, M. Kalmutzki, U. Lächelt, E. Ploetz, C. S. Diercks and S. Wuttke, *Angew. Chem., Int. Ed.*, 2021, **60**, 23975–24001.
- K. Li, J. Yang and J. Gu, *Acc. Chem. Res.*, 2022, **55**, 2235–2247.
- X.-L. Lv, S. Yuan, L.-H. Xie, H. F. Darke, Y. Chen, T. He, C. Dong, B. Wang, Y.-Z. Zhang, J.-R. Li and H.-C. Zhou, *J. Am. Chem. Soc.*, 2019, **141**, 10283–10293.
- I. Ahmed, Md. M. H. Mondol, M. Jung, G. H. Lee and S. H. Jhung, *Coord. Chem. Rev.*, 2023, **475**, 214912.
- S. Yuan, P. Zhang, L. Zhang, A. T. Garcia-Esparza, D. Sokaras, J.-S. Qin, L. Feng, G. S. Day, W. Chen, H. F. Drake, P. Elumalai, S. T. Madrahimov, D. Sun and H.-C. Zhou, *J. Am. Chem. Soc.*, 2018, **140**, 10814–10819.
- X. Fang, B. Zong and S. Mao, *Nano-Micro Lett.*, 2018, **10**, 64.
- Z. J. Gartner and J. L. Hu, *Nat. Mater.*, 2021, **20**, 2–3.
- Y. Qian, F. Zhang and H. Pang, *Adv. Funct. Mater.*, 2021, **31**, 2104231.
- B. Bayatsarmadi, Y. Zheng, A. Vasileff and S.-Z. Qiao, *Small*, 2017, **13**, 1700191.
- S. Rezaee and S. Shahrokhian, *Appl. Catal., B*, 2019, **244**, 802–813.
- J. A. Cruz-Navarro, F. Hernandez-Garcia and G. A. Alvarez Romero, *Coord. Chem. Rev.*, 2020, **412**, 213263.
- H. Yang, S. J. Bradley, A. Chan, G. I. N. Waterhouse, T. Nann, P. E. Kruger and S. G. Telfer, *J. Am. Chem. Soc.*, 2016, **138**, 11872–11881.
- Y.-C. Han, M.-L. Liu, L. Sun, X.-C. Li, Y. Yao, C. Zhang, S.-Y. Ding, H.-G. Liao, L. Zhang, F. R. Fan, M. Moskovits and Z.-Q. Tian, *Nano Energy*, 2022, **97**, 107125.
- J. Tang and Y. Yamauchi, *Nat. Chem.*, 2016, **8**, 638–639.
- J. Duan, Y. Sun, S. Chen, X. Chen and C. Zhao, *J. Mater. Chem. A*, 2020, **8**, 18810–18815.
- M. Muschi and C. Serre, *Coord. Chem. Rev.*, 2019, **387**, 262–272.
- C.-L. Zhang, Y. Xie, J.-T. Liu, F.-H. Cao, H.-P. Cong and H. Li, *Chem. Eng. J.*, 2021, **419**, 129977.
- Y. Lu, C. Liu, C. Mei, J. Sun, J. Lee, Q. Wu, M. A. Hubbe and M.-C. Li, *Coord. Chem. Rev.*, 2022, **461**, 214496.
- X. Zhang and A. Beyer, *Nanoscale*, 2021, **13**, 1443–1484.
- H. Wei, Y. Tian, Q. Chen, D. Estevez, P. Xu, H.-X. Peng and F. Qin, *Chem. Eng. J.*, 2021, **405**, 126637.
- J. Yu, C. Mu, B. Yan, X. Qin, C. Shen, H. Xue and H. Pang, *Mater. Horiz.*, 2017, **4**, 557–569.
- H. Sun, B. Tang and P. Wu, *ACS Appl. Mater. Interfaces*, 2017, **9**, 35075–35085.
- R. Wang, D. Jin, Y. Zhang, S. Wang, J. Lang, X. Yan and L. Zhang, *J. Mater. Chem. A*, 2016, **5**, 292–302.
- S. Liu, T. Zhao, X. Tan, L. Guo, J. Wu, X. Kang, H. Wang, L. Sun and W. Chu, *Nano Energy*, 2019, **63**, 103894.
- S. Mubarak, D. Dharmodharan, P. N. P. Ghoderao and H.-S. Byun, *Coord. Chem. Rev.*, 2022, **471**, 214741.

- 54 L. Song, X. Cao, L. Li, Q. Wang, H. Ye, L. Gu, C. Mao, J. Song, S. Zhang and H. Niu, *Adv. Funct. Mater.*, 2017, **27**, 1700474.
- 55 F. Li, J. Jiang, J. Wang, J. Zou, W. Sun, H. Wang, K. Xiang, P. Wu and J.-P. Hsu, *Nano Res.*, 2023, **16**, 127–145.
- 56 C. Han, Q. Li, D. Wang, Q. Lu, Z. Xing and X. Yang, *Small*, 2018, **14**, 1703642.
- 57 W.-G. Cui, X.-Y. Zhuang, Y.-T. Li, H. Zhang, J.-J. Dai, L. Zhou, Z. Hu and T.-L. Hu, *Appl. Catal., B*, 2021, **287**, 119959.
- 58 C. Zheng, X. Qiu, J. Han, Y. Wu and S. Liu, *ACS Appl. Mater. Interfaces*, 2019, **11**, 42243–42249.
- 59 Y. Tan, L. Yang, D. Zhai, L. Sun, S. Zhai, W. Zhou, X. Wang, W.-Q. Deng and H. Wu, *Small*, 2022, **18**, 2204942.
- 60 X. Li, N. Wang, X. Bao, Q. Li, J. Li, Y.-B. Xie, S. Ji, J. Yuan and Q.-F. An, *J. Mater. Chem. A*, 2020, **8**, 17212–17218.
- 61 J. Xue, C. Han, Y. Yang, S. Xu, Q. Li, H. Nie, J. Qian and Z. Yang, *Inorg. Chem.*, 2023, **62**, 3288–3296.
- 62 Y. Xu, W. Tu, B. Zhang, S. Yin, Y. Huang, M. Kraft and R. Xu, *Adv. Mater.*, 2017, **29**, 1605957.
- 63 X. Duan, J. Kang, W. Tian, H. Zhang, S.-H. Ho, Y.-A. Zhu, Z. Ao, H. Sun and S. Wang, *Appl. Catal., B*, 2019, **256**, 117795.
- 64 L. Wang, M. Huang, X. Yu, W. You, J. Zhang, X. Liu, M. Wang and R. Che, *Nano-Micro Lett.*, 2020, **12**, 150.
- 65 H. Zhang, W. Zhang and F. Huang, *Chem. Eng. J.*, 2022, **434**, 134503.
- 66 T. Shiraki, Y. Miyauchi, K. Matsuda and N. Nakashima, *Acc. Chem. Res.*, 2020, **53**, 1846–1859.
- 67 S. Li, Z. Zheng, S. Liu, Z. Chi, X. Chen, Y. Zhang and J. Xu, *Chem. Eng. J.*, 2022, **430**, 132530.
- 68 J. Wang and H. C. Zeng, *ACS Appl. Mater. Interfaces*, 2020, **12**, 50324–50332.
- 69 M. W. Chung, C. H. Choi, S. Y. Lee and S. I. Woo, *Nano Energy*, 2015, **11**, 526–532.
- 70 J. Wang, W. Zang, S. Xi, M. Kosari, S. J. Pennycook and H. C. Zeng, *J. Mater. Chem. A*, 2020, **8**, 17266–17275.
- 71 R. B. González-González, A. Sharma, R. Parra-Saldívar, R. A. Ramírez-Mendoza, M. Bilal and H. M. N. Iqbal, *J. Hazard. Mater.*, 2022, **423**, 127145.
- 72 F. Zhang, S. Yin, Y. Chen, Q. Zheng, L. Wang and W. Jiang, *Chem. Eng. J.*, 2022, **433**, 133586.
- 73 B.-X. Zhou, S.-S. Ding, B.-J. Zhang, L. Xu, R.-S. Chen, L. Luo, W.-Q. Huang, Z. Xie, A. Pan and G.-F. Huang, *Appl. Catal., B*, 2019, **254**, 321–328.
- 74 R. Cheng, M. Jiang, K. Li, M. Guo, J. Zhang, J. Ren, P. Meng, R. Li and C. Fu, *Chem. Eng. J.*, 2021, **425**, 130603.
- 75 R. Lin, L. Ge, H. Diao, V. Rudolph and Z. Zhu, *J. Mater. Chem. A*, 2016, **4**, 6084–6090.
- 76 I. Jarchum, *Nat. Methods*, 2014, **11**, 1194.
- 77 C. Sealy, *Nano Today*, 2017, **13**, 1–2.
- 78 Y. Liu, G. Li, Y. Guo, Y. Ying and X. Peng, *ACS Appl. Mater. Interfaces*, 2017, **9**, 14043–14050.
- 79 X. Wang, A. Dong, Y. Hu, J. Qian and S. Huang, *Chem. Commun.*, 2020, **56**, 10809–10823.
- 80 L. Zou, C.-C. Hou, Z. Liu, H. Pang and Q. Xu, *J. Am. Chem. Soc.*, 2018, **140**, 15393–15401.
- 81 X. Song, S. Chen, L. Guo, Y. Sun, X. Li, X. Cao, Z. Wang, J. Sun, C. Lin and Y. Wang, *Adv. Energy Mater.*, 2018, **8**, 1801101.
- 82 W. Zhang, P. Cao, Z. Zhang, Y. Zhao, Y. Zhang, L. Li, K. Yang, X. Li and L. Gu, *Chem. Eng. J.*, 2019, **364**, 123–131.
- 83 X. Yang, X. Jiang, Y. Huang, Z. Guo and L. Shao, *ACS Appl. Mater. Interfaces*, 2017, **9**, 5590–5599.
- 84 F. Yang, P. Zhao, X. Hua, W. Luo, G. Cheng, W. Xing and S. Chen, *J. Mater. Chem. A*, 2016, **4**, 16057–16063.
- 85 J. Meng, C. Niu, L. Xu, J. Li, X. Liu, X. Wang, Y. Wu, X. Xu, W. Chen, Q. Li, Z. Zhu, D. Zhao and L. Mai, *J. Am. Chem. Soc.*, 2017, **139**, 8212–8221.
- 86 A. Magrez, R. Smajda, J. W. Seo, E. Horváth, P. R. Ribic, J. C. Andresen, D. Acquaviva, A. Olariu, G. Laurenczy and L. Forró, *ACS Nano*, 2011, **5**, 3428–3437.
- 87 S.-K. Park, J. K. Kim and Y. C. Kang, *Chem. Eng. J.*, 2017, **328**, 546–555.
- 88 H. T. T. Pham, Y. Kim, Y.-J. Kim, J.-W. Lee and M.-S. Park, *Adv. Funct. Mater.*, 2019, **29**, 1902915.
- 89 D. Micheroni, G. Lan and W. Lin, *J. Am. Chem. Soc.*, 2018, **140**, 15591–15595.
- 90 H. Zhang, W. Zhao, Y. Wu, Y. Wang, M. Zou and A. Cao, *J. Mater. Chem. A*, 2019, **7**, 9195–9201.
- 91 D. Chen, Q. Sun, C. Han, Y. Guo, Q. Huang, W. A. Goddard and J. Qian, *J. Mater. Chem. A*, 2022, **10**, 16007–16015.
- 92 J. Lin, C. Zeng, X. Lin, C. Xu and C. Su, *Adv. Sci.*, 2020, **7**, 2000736.
- 93 Y. Pan, K. Sun, S. Liu, X. Cao, K. Wu, W.-C. Cheong, Z. Chen, Y. Wang, Y. Li, Y. Liu, D. Wang, Q. Peng, C. Chen and Y. Li, *J. Am. Chem. Soc.*, 2018, **140**, 2610–2618.
- 94 H. Park, S. Oh, S. Lee, S. Choi and M. Oh, *Appl. Catal., B*, 2019, **246**, 322–329.
- 95 L. Chai, Z. Hu, X. Wang, Y. Xu, L. Zhang, T. Li, Y. Hu, J. Qian and S. Huang, *Adv. Sci.*, 2020, **7**, 1903195.
- 96 Y. Zhou, X. Deng, H. Xing, H. Zhao, Y. Liu, L. Guo, J. Feng, W. Feng, Y. Zong, X. Zhu, X. Li, Y. Peng and X. Zheng, *Nano Res.*, 2022, **15**, 6819–6830.
- 97 Y. Wu, G. Liang, D. Chen, Z. Li, J. Xu, G. Huang, M. Yang, H. Zhang, J. Chen, F. Xie, Y. Jin, N. Wang, S. Sun and H. Meng, *ACS Appl. Mater. Interfaces*, 2021, **13**, 48923–48933.
- 98 S. Fan, S. Huang, Y. Chen, Y. Shang, Y. Wang, D. Kong, M. E. Pam, L. Shi, Y. W. Lim, Y. Shi and H. Y. Yang, *Energy Storage Mater.*, 2019, **23**, 17–24.
- 99 Y. Xie, C. Feng, Y. Guo, S. Li, C. Guo, Y. Zhang and J. Wang, *Appl. Surf. Sci.*, 2021, **536**, 147786.
- 100 X. Chen, N. Wang, K. Shen, Y. Xie, Y. Tan and Y. Li, *ACS Appl. Mater. Interfaces*, 2019, **11**, 25976–25985.
- 101 D. D. Chronopoulos, H. Saini, I. Tantis, R. Zbořil, K. Jayaramulu and M. Otyepka, *Small*, 2022, **18**, 2104628.
- 102 Y.-L. Wang, P.-Y. Zhao, B.-L. Liang, K. Chen and G.-S. Wang, *Carbon*, 2023, **202**, 66–75.
- 103 Q. Ren, T. Feng, Z. Song, P. Zhou, M. Wang, Q. Zhang and L. Wang, *ACS Appl. Mater. Interfaces*, 2022, **14**, 41246–41256.
- 104 W. Xue, G. Yang, S. Bi, J. Zhang and Z.-L. Hou, *Carbon*, 2021, **173**, 521–527.
- 105 H. Yang and X. Wang, *Adv. Mater.*, 2019, **31**, 1800743.

- 106 F. Wang, L. Hu, R. Liu, H. Yang, T. Xiong, Y. Mao, M.-S. J. T. Balogun, G. Ouyang and Y. Tong, *J. Mater. Chem. A*, 2019, **7**, 11150–11159.
- 107 Y. Guo, Q. Sun, Q. Huang, Y. Hu, K. Su, T.-T. Li, S. Huang and J. Qian, *Carbon*, 2022, **196**, 457–465.
- 108 T. Wang, H.-K. Kim, Y. Liu, W. Li, J. T. Griffiths, Y. Wu, S. Laha, K. D. Fong, F. Podjaski, C. Yun, R. V. Kumar, B. V. Lotsch, A. K. Cheetham and S. K. Smoukov, *J. Am. Chem. Soc.*, 2018, **140**, 6130–6136.
- 109 S. Chen, M. Li, M. Zhang, C. Wang, R. Luo, X. Yan, H. Zhang, J. Qi, X. Sun and J. Li, *J. Hazard. Mater.*, 2021, **416**, 126101.
- 110 J. Zhou, G. Zhang, J. Luo, Y. Hu, G. Hao, H. Guo, F. Guo, S. Wang and W. Jiang, *Chem. Eng. J.*, 2021, **426**, 130725.
- 111 W. Zhang, X. Yao, S. Zhou, X. Li, L. Li, Z. Yu and L. Gu, *Small*, 2018, **14**, 1800423.
- 112 L. Zou, M. Kitta, J. Hong, K. Suenaga, N. Tsumori, Z. Liu and Q. Xu, *Adv. Mater.*, 2019, 1900440.
- 113 A. G. Slater, M. A. Little, A. Pulido, S. Y. Chong, D. Holden, L. Chen, C. Morgan, X. Wu, G. Cheng, R. Clowes, M. E. Briggs, T. Hasell, K. E. Jelfs, G. M. Day and A. I. Cooper, *Nat. Chem.*, 2017, **9**, 17–25.
- 114 H. Lu, C. Zhang, Y. Zhang, Y. Huang, M. Liu and T. Liu, *Nano Res.*, 2018, **11**, 6155–6166.
- 115 B. Liu, K. Vellingiri, S.-H. Jo, P. Kumar, Y. S. Ok and K.-H. Kim, *Nano Res.*, 2018, **11**, 4441–4467.
- 116 J. Kim, C. Young, J. Lee, Y.-U. Heo, M.-S. Park, Md. S. A. Hossain, Y. Yamauchi and J. H. Kim, *J. Mater. Chem. A*, 2017, **5**, 15065–15072.
- 117 H. Zhong, Y. Luo, S. He, P. Tang, D. Li, N. Alonso-Vante and Y. Feng, *ACS Appl. Mater. Interfaces*, 2017, **9**, 2541–2549.
- 118 Z. Yang, L. Zhang, Y. Zhang, M. Bai, Y. Zhang, Z. Yue and E. Duan, *Chem. Eng. J.*, 2020, **395**, 124980.
- 119 K. Tian, J. Wang, L. Cao, W. Yang, W. Guo, S. Liu, W. Li, F. Wang, X. Li, Z. Xu, Z. Wang, H. Wang and Y. Hou, *Nat. Commun.*, 2020, **11**, 3884.
- 120 Y. Zou, X. Zhou, Y. Zhu, X. Cheng, D. Zhao and Y. Deng, *Acc. Chem. Res.*, 2019, **52**, 714–725.
- 121 C. Preischl, L. H. Le, E. Bilgiliyoy, F. Vollnhals, A. Götzhäuser and H. Marbach, *Small*, 2020, **16**, 2003947.
- 122 X. Zhou and G. Yu, *Adv. Mater.*, 2020, **32**, 1905957.
- 123 H. Ang and L. Hong, *ACS Appl. Mater. Interfaces*, 2017, **9**, 28079–28088.
- 124 M. Cai, Q. Liu, Z. Xue, Y. Li, Y. Fan, A. Huang, M.-R. Li, M. Croft, T. A. Tyson, Z. Ke and G. Li, *J. Mater. Chem. A*, 2020, **8**, 190–195.
- 125 Q. Huang, Y. Xu, Y. Guo, L. Zhang, Y. Hu, J. Qian and S. Huang, *Carbon*, 2022, **188**, 135–145.
- 126 P. He, Y. Xie, Y. Dou, J. Zhou, A. Zhou, X. Wei and J.-R. Li, *ACS Appl. Mater. Interfaces*, 2019, **11**, 41595–41601.
- 127 A. Goswami, D. Ghosh, V. V. Chernyshev, A. Dey, D. Pradhan and K. Biradha, *ACS Appl. Mater. Interfaces*, 2020, **12**, 33679–33689.
- 128 R. Wei, Y. Gu, L. Zou, B. Xi, Y. Zhao, Y. Ma, Y. Qian, S. Xiong and Q. Xu, *Nano Lett.*, 2020, **20**, 7342–7349.
- 129 P. Pachfule, D. Shinde, M. Majumder and Q. Xu, *Nat. Chem.*, 2016, **8**, 718–724.
- 130 W. Xia, J. Tang, J. Li, S. Zhang, K. C. -W. Wu, J. He and Y. Yamauchi, *Angew. Chem.*, 2019, **131**, 13488–13493.
- 131 J. Y. Choi, J. Flood, M. Stodolka, H. T. B. Pham and J. Park, *ACS Nano*, 2022, **16**, 3145–3151.
- 132 Q. Li, Y. Zhao, X. Li, L. Wang, X. Li, J. Zhang and R. Che, *Small*, 2020, **16**, 2003905.
- 133 L. Yang, H. Li, Y. Yu, Y. Wu and L. Zhang, *Appl. Catal., B*, 2020, **271**, 118939.
- 134 X. Xu, F. Ran, H. Lai, Z. Cheng, T. Lv, L. Shao and Y. Liu, *ACS Appl. Mater. Interfaces*, 2019, **11**, 35999–36009.
- 135 Y. Wang, Y. Gao, J. Shao, R. Holze, Z. Chen, Y. Yun, Q. Qu and H. Zheng, *J. Mater. Chem. A*, 2018, **6**, 3659–3666.
- 136 Y. Wang, L. Tao, Z. Xiao, R. Chen, Z. Jiang and S. Wang, *Adv. Funct. Mater.*, 2018, **28**, 1705356.
- 137 Z. Lv, X. Tan, C. Wang, A. Alsaedi, T. Hayat and C. Chen, *Chem. Eng. J.*, 2020, **389**, 123428.
- 138 H. S. Kim, M. S. Kang and W. C. Yoo, *J. Mater. Chem. A*, 2019, **7**, 5561–5574.
- 139 W. Chen, J. Pei, C.-T. He, J. Wan, H. Ren, Y. Wang, J. Dong, K. Wu, W.-C. Cheong, J. Mao, X. Zheng, W. Yan, Z. Zhuang, C. Chen, Q. Peng, D. Wang and Y. Li, *Adv. Mater.*, 2018, **30**, 1800396.
- 140 Z. Ye, J. A. Padilla, E. Xuriguera, E. Brillas and I. Sirés, *Appl. Catal., B*, 2020, **266**, 118604.
- 141 X. F. Lu, L. Yu, J. Zhang and X. W. (David) Lou, *Adv. Mater.*, 2019, 1900699.
- 142 H. Hong, J. Liu, H. Huang, C. Atangana Etogo, X. Yang, B. Guan and L. Zhang, *J. Am. Chem. Soc.*, 2019, **141**, 14764–14771.
- 143 J. Kim, J. Kim, J. H. Kim and H. S. Park, *Chem. Eng. J.*, 2020, **382**, 122996.
- 144 L. Qi, Y. Xin, Z. Zuo, C. Yang, K. Wu, B. Wu and H. Zhou, *ACS Appl. Mater. Interfaces*, 2016, **8**, 17245–17252.
- 145 D. Cao, W. Kang, W. Wang, K. Sun, Y. Wang, P. Ma and D. Sun, *Small*, 2020, **16**, 1907641.
- 146 Z. Cai, Z. Wang, J. Kim and Y. Yamauchi, *Adv. Mater.*, 2019, **31**, 1804903.
- 147 K.-Y. Andrew Lin, H.-A. Chang and B.-J. Chen, *J. Mater. Chem. A*, 2016, **4**, 13611–13625.
- 148 M.-L. Xu, X.-J. Jiang, J.-R. Li, F.-J. Wang, K. Li and X. Cheng, *ACS Appl. Mater. Interfaces*, 2021, **13**, 56171–56180.
- 149 S. Li, Y. Hou, Q. Chen, X. Zhang, H. Cao and Y. Huang, *ACS Appl. Mater. Interfaces*, 2020, **12**, 2581–2590.
- 150 X. Wang, L. Chai, J. Ding, L. Zhong, Y. Du, T.-T. Li, Y. Hu, J. Qian and S. Huang, *Nano Energy*, 2019, **62**, 745–753.
- 151 Y. Dong, J. Li and L. Zhang, *Sens. Actuators, B*, 2020, **303**, 127208.
- 152 J. Sheng, L. Wang, L. Deng, M. Zhang, H. He, K. Zeng, F. Tang and Y.-N. Liu, *ACS Appl. Mater. Interfaces*, 2018, **10**, 7191–7200.
- 153 S. Sun, X. Sun, Y. Liu, J. Peng, Y. Qiu, Y. Xu, J. Zhang, Q. Li, C. Fang, J. Han and Y. Huang, *J. Mater. Chem. A*, 2019, **7**, 17248–17253.
- 154 J. Yang, S. Xiao, X. Cui, W. Dai, X. Lian, Z. Hao, Y. Zhao, J.-S. Pan, Y. Zhou, L. Wang and W. Chen, *Energy Storage Mater.*, 2020, **26**, 391–399.

- 155 P. He, Y. Wu, H. Chen, Z. Zhu, H. Liu, J. Gao and H. Xu, *J. Alloys Compd.*, 2020, **813**, 152192.
- 156 R. Gao, J. Tang, X. Yu, S. Tang, K. Ozawa, T. Sasaki and L.-C. Qin, *Nano Energy*, 2020, **70**, 104444.
- 157 C.-L. Zhang, J.-T. Liu, H. Li, L. Qin, F.-H. Cao and W. Zhang, *Appl. Catal., B*, 2020, **261**, 118224.
- 158 L. Yan, Y. Xu, P. Chen, S. Zhang, H. Jiang, L. Yang, Y. Wang, L. Zhang, J. Shen, X. Zhao and L. Wang, *Adv. Mater.*, 2020, **32**, 2003313.
- 159 R. Yuksel, O. Buyukcakir, P. K. Panda, S. H. Lee, Y. Jiang, D. Singh, S. Hansen, R. Adelung, Y. K. Mishra, R. Ahuja and R. S. Ruoff, *Adv. Funct. Mater.*, 2020, **30**, 1909725.
- 160 X. Zhang, Y. Wei, B. Wang, M. Wang, Y. Zhang, Q. Wang and H. Wu, *Nano-Micro Lett.*, 2019, **11**, 78.
- 161 A. Lv, S. Lu, M. Wang, H. Shi, W. Yan and S. Jiao, *J. Energy Chem.*, 2022, **69**, 35–43.
- 162 S. C. Hess, R. N. Grass and W. J. Stark, *Chem. Mater.*, 2016, **28**, 7638–7644.
- 163 T. Y. Yoo, J. M. Yoo, A. K. Sinha, M. S. Bootharaju, E. Jung, H. S. Lee, B.-H. Lee, J. Kim, W. H. Antink, Y. M. Kim, J. Lee, E. Lee, D. W. Lee, S.-P. Cho, S. J. Yoo, Y.-E. Sung and T. Hyeon, *J. Am. Chem. Soc.*, 2020, **142**, 14190–14200.
- 164 X. Wang, Y. Fei, W. Li, L. Yi, B. Feng, Y. Pan, W. Hu and C. M. Li, *ACS Appl. Mater. Interfaces*, 2020, **12**, 16548–16556.
- 165 J. Li, P. Liu, J. Mao, J. Yan and W. Song, *J. Mater. Chem. A*, 2021, **9**, 11248–11254.
- 166 H. Wang, *Nano Res.*, 2022, **15**, 2834–2854.
- 167 B. Li, K. Igawa, J. Chai, Y. Chen, Y. Wang, D. W. Fam, N. N. Tham, T. An, T. Konno, A. Sng, Z. Liu, H. Zhang and Y. Zong, *Energy Storage Mater.*, 2020, **25**, 137–144.
- 168 Y. Zhao, L. Zheng, D. Jiang, W. Xia, X. Xu, Y. Yamauchi, J. Ge and J. Tang, *Small*, 2021, **17**, 2006590.
- 169 R. M. Rego, G. Kuriya, M. D. Kurkuri and M. Kigga, *J. Hazard. Mater.*, 2021, **403**, 123605.
- 170 G. Zou, H. Hou, P. Ge, Z. Huang, G. Zhao, D. Yin and X. Ji, *Small*, 2018, **14**, 1702648.
- 171 Y.-Z. Chen, R. Zhang, L. Jiao and H.-L. Jiang, *Coord. Chem. Rev.*, 2018, **362**, 1–23.
- 172 Z. Liang, C. Qu, D. Xia, R. Zou and Q. Xu, *Angew. Chem., Int. Ed.*, 2018, **57**, 9604–9633.
- 173 A. Indra, T. Song and U. Paik, *Adv. Mater.*, 2018, **30**, 1705146.
- 174 X. Qin, D. Kim and Y. Piao, *Carbon Energy*, 2021, **3**, 66–100.
- 175 R. Liu, X.-R. Shi, Y. Wen, X. Shao, C. Su, J. Hu and S. Xu, *J. Energy Chem.*, 2022, **74**, 149–158.
- 176 L. Li, N. Li, J. Xia, S. Zhou, X. Qian, F. Yin, G. He and H. Chen, *J. Mater. Chem. A*, 2023, **11**, 2291–2301.
- 177 Y.-C. Wang, J.-H. Yen, C.-W. Huang, T.-E. Chang, Y.-L. Chen, Y.-H. Chen, C.-Y. Lin and C.-W. Kung, *ACS Appl. Mater. Interfaces*, 2022, **14**, 35534–35544.
- 178 P.-Y. Zhang, X.-H. Yang, Q.-R. Jiang, P.-X. Cui, Z.-Y. Zhou, S.-H. Sun, Y.-C. Wang and S.-G. Sun, *ACS Appl. Mater. Interfaces*, 2022, **14**, 30724–30734.
- 179 S. Saifi, G. Dey, J. Karthikeyan, A. S. K. Sinha and A. Aijaz, *ACS Appl. Nano Mater.*, 2022, **5**, 10696–10703.
- 180 X. Xie, L. Shang, X. Xiong, R. Shi and T. Zhang, *Adv. Energy Mater.*, 2022, **12**, 2102688.
- 181 M. Kim, K. L. Firestein, J. F. S. Fernando, X. Xu, H. Lim, D. V. Golberg, J. Na, J. Kim, H. Nara, J. Tang and Y. Yamauchi, *Chem. Sci.*, 2022, **13**, 10836–10845.
- 182 B. Chen, L. Chen, L. Zu, Y. Feng, Q. Su, C. Zhang and J. Yang, *Adv. Mater.*, 2022, **34**, 2200894.
- 183 D. Geng, S. Zhang, Y. Jiang, Z. Jiang, M. Shi, J. Chang, S. Liang, M. Zhang, J. Feng, T. Wei and Z. Fan, *J. Mater. Chem. A*, 2022, **10**, 2027–2034.
- 184 Z. Kong, L. Wang, S. Iqbal, B. Zhang, B. Wang, J. Dou, F. Wang, Y. Qian, M. Zhang and L. Xu, *Small*, 2022, **18**, 2107252.
- 185 Y. Li, H. Xie, J. Li, Y. Yamauchi and J. Henzie, *ACS Appl. Mater. Interfaces*, 2021, **13**, 41649–41656.
- 186 R. Muruganatham, Y.-J. Gu, Y.-D. Song, C.-W. Kung and W.-R. Liu, *Appl. Mater. Today*, 2021, **22**, 100935.
- 187 N. Kumar, N. Bansal, Y. Yamauchi and R. R. Salunkhe, *Chem. Mater.*, 2022, **34**, 4946–4954.
- 188 Y. Wang, J. Li, X. Li, H. Jin, W. Ali, Z. Song and S. Ding, *J. Mater. Chem. A*, 2022, **10**, 699–706.
- 189 X. Liao, X. Zhang, W. Wang, C. Liu, W. Yang and D. Wang, *Biosens. Bioelectron.*, 2023, **220**, 114906.
- 190 P. Iacomini, E. Gulcay-Ozcan, P. Pires Conti, S. Biswas, N. Steunou, G. Maurin, G. Riolland and S. Devautour-Vinot, *ACS Appl. Mater. Interfaces*, 2022, **14**, 17531–17538.
- 191 Z. Qi and Y. Chen, *Biosens. Bioelectron.*, 2017, **87**, 236–241.
- 192 J. F. Olorunyomi, J. F. White, T. R. Gengenbach, R. A. Caruso and C. M. Doherty, *ACS Appl. Mater. Interfaces*, 2022, **14**, 35755–35768.
- 193 F. Zhang, Z. Jia, J. Zhou, J. Liu, G. Wu and P. Yin, *Chem. Eng. J.*, 2022, **450**, 138205.
- 194 C. Xiong, L. Tian, C. Xiao, Z. Xue, F. Zhou, H. Zhou, Y. Zhao, M. Chen, Q. Wang, Y. Qu, Y. Hu, W. Wang, Y. Zhang, X. Zhou, Z. Wang, P. Yin, Y. Mao, Z.-Q. Yu, Y. Cao, X. Duan, L. Zheng and Y. Wu, *Sci. Bull.*, 2020, **65**, 2100–2106.
- 195 H. Li, L. Su, J. Zheng, S. Lu, Z. Yang, C. Wang, S. Xu, Q. Zhou, J. Tang, M. Huang and Y. Zhang, *Chem. Eng. J.*, 2023, **451**, 139114.